Author Manuscript

Author Manuscript

Author Manuscript

Author Manuscript

HHS Public Access

Author manuscript

Neuroimage. Author manuscript; available in PMC 2018 May 15.

Published in final edited form as:

Neuroimage. 2017 May 15; 152: 78–93. doi:10.1016/j.neuroimage.2017.02.061.

Electrocorticographic delineation of human auditory cortical fields based on effects of propofol anesthesia

Kirill V. Nourski[1], **Matthew I. Banks**[2], **Mitchell Steinschneider**[3], **Ariane E. Rhone**[1], **Hiroto Kawasaki**[1], **Rashmi N. Mueller**[4], **Michael M. Todd**[4,5], and **Matthew A. Howard III**[1,6,7]

[1]Department of Neurosurgery, The University of Iowa, Iowa City, IA, USA

[2]Department of Anesthesiology, University of Wisconsin – Madison, Madison, WI, USA

[3]Departments of Neurology and Neuroscience, Albert Einstein College of Medicine, Bronx, NY, USA

[4]Department of Anesthesia, The University of Iowa, Iowa City, IA, USA

[5]Department of Anesthesiology, University of Minnesota, Minnesota, MN USA

[6]Pappajohn Biomedical Institute, The University of Iowa, Iowa City, IA, USA

[7]Iowa Neuroscience Institute, The University of Iowa, Iowa City, IA, USA

Abstract

The functional organization of human auditory cortex remains incompletely characterized. While the posteromedial two thirds of Heschl's gyrus (HG) is generally considered to be part of core auditory cortex, additional subdivisions of HG remain speculative. To further delineate the hierarchical organization of human auditory cortex, we investigated regional heterogeneity in the modulation of auditory cortical responses under varying depths of anesthesia induced by propofol. Non-invasive studies have shown that propofol differentially affects auditory cortical activity, with a greater impact on non-core areas. Subjects were neurosurgical patients undergoing removal of intracranial electrodes placed to identify epileptic foci. Stimuli were 50 Hz click trains, presented continuously during an awake baseline period, and subsequently, while propofol infusion was incrementally titrated to induce general anesthesia. Electrocorticographic recordings were made with depth electrodes implanted in HG and subdural grid electrodes implanted over superior temporal gyrus (STG). Depth of anesthesia was monitored using spectral entropy. Averaged evoked potentials (AEPs), frequency-following responses (FFRs) and high gamma (70–150 Hz) event-related band power (ERBP) were used to characterize auditory cortical activity. Based on the changes in AEPs and FFRs during the induction of anesthesia, posteromedial HG could be divided into two subdivisions. In the most posteromedial aspect of the gyrus, the earliest AEP deflections were preserved and FFRs increased during induction. In contrast, the remainder of the

Corresponding Author: Kirill V. Nourski, MD, PhD, Department of Neurosurgery, The University of Iowa, 200 Hawkins Dr. 1815 JCP, Iowa City, IA 52242-1061 USA, Phone: +1 (319) 335-7049, Fax: +1 (319) 335-6605, kirill-nourski@uiowa.edu.

Publisher's Disclaimer: This is a PDF file of an unedited manuscript that has been accepted for publication. As a service to our customers we are providing this early version of the manuscript. The manuscript will undergo copyediting, typesetting, and review of the resulting proof before it is published in its final citable form. Please note that during the production process errors may be discovered which could affect the content, and all legal disclaimers that apply to the journal pertain.

Author Manuscript Author Manuscript Author Manuscript Author Manuscript

posteromedial HG exhibited attenuation of both the AEP and the FFR. The anterolateral HG exhibited weaker activation characterized by broad, low-voltage AEPs and the absence of FFRs. Lateral STG exhibited limited activation by click trains, and FFRs there diminished during induction. Sustained high gamma activity was attenuated in the most posteromedial portion of HG, and was absent in all other regions. These differential patterns of auditory cortical activity during the induction of anesthesia may serve as useful physiological markers for field delineation. In this study, the posteromedial HG could be parcellated into at least two subdivisions. Preservation of the earliest AEP deflections and FFRs in the posteromedial HG likely reflects the persistence of feedforward synaptic activity generated by inputs from subcortical auditory pathways, including the medial geniculate nucleus.

Keywords

General anesthesia; frequency-following response; Heschl's gyrus; high gamma; intracranial recordings

1. Introduction

Delineation of auditory cortex on Heschl's gyrus (HG) remains controversial despite decades of research, (Hackett, 2007, 2015). Studies in non-human primates suggest a framework in which the auditory cortex is hierarchically organized into several core, belt and parabelt regions (Rauschecker et al., 1995; Hackett et al., 1998; Brugge and Howard, 2002; Kaas and Hackett, 2005). According to this model, primary auditory cortex (area AI) and adjacent cortex (areas R and RT) form the core region, concentrically surrounded by belt, and then parabelt regions. Most anatomical and functional neuroimaging studies in humans conclude that the posteromedial portion (approximately two thirds) of HG is comprised of core auditory cortex (e.g., Rivier and Clarke, 1997; Talavage et al., 2000; Hackett et al., 2001; Wallace et al., 2002; Sweet et al., 2005; Woods et al., 2009). However, even at the fundamental level of cytoarchitectonics, there have been a variety of interpretations of the data (reviewed in Hackett, 2007, 2015). For instance, the most posteromedial aspect of HG has been variously labeled as core (Rivier and Clarke et al., 1997; Morosan et al., 2001; Wallace et al., 2002; Sweet at el., 2005) or belt areas (Galaburda and Sanides, 1980; Fullerton and Pandya, 2007). Furthermore, the anterolateral third of HG has also been interpreted as either core (Formisano et al., 2003; Woods et al., 2010) or belt (Kaas and Hackett, 2000; Woods et al., 2009). The considerable structural complexity of the human HG at both macroscopic and microscopic levels and its inter-subject variability have hindered efforts to consolidate the results of the many mapping studies into a unified model (e.g. Zilles et al., 1997; Hackett et al., 2001; Morosan et al., 2001; Destrieux et al., 2010).

The inability to parcellate auditory cortex on HG using neuroanatomical criteria alone led to the use of physiology to define this region. Tonotopy, a fundamental attribute of core auditory cortex in experimental animals, has been used to characterize HG (e.g., Talavage et al., 2000, 2004; Formisano et al., 2003; Humphries et al., 2010; Woods et al., 2010; Da Costa et al., 2011; Striem-Amit et al., 2011; Langers and van Dijk, 2012). This approach yielded multiple configurations of tonotopic gradients with respect to the long axis of HG

Author Manuscript Author Manuscript Author Manuscript Author Manuscript

(reviewed in Baumann et al., 2013, Moerel et al., 2014; Saenz and Langers, 2015). Intracranial electrophysiology studies, with their excellent spatial and temporal resolution, have been especially useful in demarcating fields based on functional grounds (Liégeois-Chauvel et al., 1991; Howard et al., 1996; Brugge et al., 2008; Nourski et al., 2014). Responses with the shortest latency, presumably arising in core areas, consistently localize to the posteromedial tip of HG (Liégeois-Chauvel et al., 1991; 1994; Yvert et al., 2005; Nourski et al., 2014). The ability to phase lock to repetitive transients is also used as a physiological marker for field demarcation, and the posteromedial portion of HG is characterized by the highest phase-locking capacity (Liégeois-Chauvel et al., 2004; Brugge et al., 2008, 2009). Integration of physiological findings with anatomy thus suggests that the most posteromedial aspect of HG is core auditory cortex. On the other hand, the caudomedial belt area CM in the macaque has been shown to exhibit core-like physiological properties, including short onset response latencies and high temporal precision (Camalier et al., 2012).

Propofol, an agent used for induction and maintenance of general anesthesia, affects cortical activity evoked by auditory stimuli (Plourde, 1996; Schwender et al., 1997; Dutton et al., 1999; Simpson et al., 2002; Heinke et al., 2004; Dueck et al., 2005; Scheller et al., 2005; Plourde et al., 2006; Davis et al., 2007), likely by modulating $GABA_A$ receptors (Bai et al., 1999; Rudolph and Antkowiak, 2004; Franks, 2008) and reducing glutamate release (Ratnakumari and Hemmings, 1997; Yang et al., 2015). Evidence suggests that during induction of anesthesia, external sensory stimuli activate the cortex but fail to be experienced (Amzica et al., 2002; Velly et al., 2007; Murphy et al., 2011; Schrouff et al., 2011; Boly et al., 2012; Schroter et al., 2012; Jordan et al., 2013).

Cortical effects of general anesthetics are region-specific and may help delineate fields on HG (e.g. Liu et al., 2011). At the thalamic level, propofol preferentially suppresses the output of non-specific (e.g. intralaminar) nuclei with relative sparing of specific thalamic nuclei (Liu et al., 2013). This distribution is consistent with minimal modulation of the ventral division (MGv) of the medial geniculate nucleus (MGN). MGv is the specific lemniscal thalamic nucleus, which projects more strongly to core than non-core auditory areas (Hashikawa et al., 1995; Molinari et al., 1995). These considerations suggest that studying the effects of propofol on activity within HG may provide new insights into its functional organization.

The effects of propofol anesthesia may also be relevant for studying and testing hypotheses regarding electrophysiological correlates of sensory awareness (Pockett, 1999). At doses of anesthesia causing loss of consciousness, stimulus-related activity in primary sensory cortex in animal models is relatively preserved, while activity in higher order areas is largely suppressed (Howard et al., 2000; Liu et al., 2011; Raz et al., 2014). This is consistent with models in which activity in core areas corresponds to pre-attentive processing (Logothetis et al., 1996; Tononi, 2004; Watanabe et al., 2011). There remains, however, considerable debate about the relationship between neural activity in primary sensory cortex and sensory perception, and these hypotheses are largely untested in the human cortex (Tong, 2003).

Author Manuscript Author Manuscript Author Manuscript Author Manuscript

Studying the differential effects of anesthesia in various regions of the auditory cortex has clinical implications. Scalp-recorded middle latency auditory evoked potentials have been proposed as a useful tool for monitoring the depth of anesthesia in clinical practice (e.g. De Cosmo et al., 2004). A more detailed understanding of the action of general anesthetics on auditory cortical activity will enhance interpretation of the changes in these responses at various depths of anesthesia. Additionally, auditory functional magnetic resonance imaging (fMRI) studies for both clinical and research purposes in infants and children often require sedation with general anesthetics. An understanding of the pharmacological properties of specific sedative agents will facilitate accurate interpretation of the information acquired by these studies (Gemma et al., 2009).

In the current study, we used electrocorticography (ECoG), which records local field potentials from neural populations in the vicinity of the electrodes (Mukamel & Fried, 2012; Nourski & Howard, 2015) to study modulation of auditory cortical activity by propofol. We have initiated our study using 50 Hz click trains, a type of auditory stimulus that produces several well-characterized response patterns that are region-specific in auditory cortex (Brugge et al., 2008, 2009; Nourski et al., 2013). The first response type is the averaged evoked potential (AEP), which is phase-locked to stimulus onsets and offsets. The second response type is sustained phase locking to the repetition rate of the click train (Brugge et al., 2009; Nourski et al., 2013). This pattern is referred to as a frequency-following response (FFR). The third response type is represented by non-phase-locked higher-frequency activity within gamma (30–70 Hz) and high gamma (70–150 Hz) frequency range. Multiple studies have demonstrated the importance of high gamma activity for auditory cortical processing (e.g. Crone et al., 2001, 2006; Brugge et al., 2009; Edwards et al., 2009; Mesgarani and Chang, 2012). Studies in non-human primates have established the high gamma band as a surrogate for unit activity (Ray et al., 2008; Steinschneider et al., 2008), while functional neuroimaging studies have demonstrated a positive correlation between high gamma activity and hemodynamic responses (Nir et al., 2007; Whittingstal and Logothetis, 2009). Thus, high gamma activity can serve as a bridge between different research techniques, facilitating comparisons across studies.

Here, we test the hypothesis that sensitivity to the anesthetic agent, propofol, can refine the parcellation of auditory fields as determined by anatomical criteria and the response to acoustic stimuli. We found that posteromedial HG can be further delineated into at least two subdivisions based on its sensitivity to propofol. Furthermore, we suggest that the continued presence of the earliest AEP deflections and FFRs under anesthesia reflects the persistence of feedforward synaptic activity arising in the MGv.

2. Methods

2.1. Subjects

Study subjects were ten neurosurgical patients (5 female, ages 27–51 years old, median age 35 years old) with medically refractory epilepsy who had been implanted with intracranial ECoG electrodes. The electrodes were used during a period of inpatient monitoring to identify resectable seizure foc. The anesthesia experiments described in this report were conducted when the patients returned to the operating room to undergo electrode removal

Author Manuscript Author Manuscript Author Manuscript Author Manuscript

and seizure focus resection surgery. The demographic and seizure focus data for each subject are presented in Table 1. Intracranial recordings established that auditory cortical areas within HG were not epileptic foci in any subject.

All subjects were native English speakers except subject R331, a native Sudanese Ma'di speaker who learned English in childhood. All subjects except two (L258 and L282) had pure-tone thresholds within 25 dB hearing level (HL) between 250 Hz and 4 kHz. Subject L258 had a mild low-frequency hearing loss (at 250 Hz, thresholds were 25 and 30 dB HL for right and left ear, respectively). Subject L282 had a moderate (55 dB) 4 kHz notch in both ears. Word recognition scores, as evaluated by spondees presented via monitored live voice, were 96/100% (right/left ear) in subject R316, 96/92% in subject R330, 92/96% in subject R331, and 100% in all other tested subjects. Speech reception thresholds were within 15 dB HL in all tested subjects, including the two with tone audiometry thresholds outside the 25 dB HL criterion.

Research protocols were approved by the University of Iowa Institutional Review Board and the National Institutes of Health, and written informed consent was obtained from all subjects. Research participation did not interfere with acquisition of clinically necessary data, and subjects could rescind consent for research without interrupting their clinical management.

2.2. Stimulus and procedure

Stimulus generation and ECoG data acquisition were controlled by a TDT RZ2 real-time processor (Tucker-Davis Technologies, Alachua, FL). The stimulus was a 500 ms train of acoustic clicks, generated digitally as 0.2 ms wide rectangular pulses and presented at a rate of 50 Hz. The interstimulus interval varied within a Gaussian distribution (onset-to-onset mean 1500 ms, S.D. = 10 ms) to reduce heterodyning in the recordings secondary to power line noise. The click trains were delivered to both ears via insert earphones (ER4B, Etymotic Research, Elk Grove Village, IL) that were integrated into custom-fit earmolds. Acoustic stimulation was performed at a comfortable level, typically 60–65 dB SPL. The stimulus was presented in a passive-listening paradigm, without any task direction.

Click trains were continuously presented in the operating room, beginning 10 minutes prior to administration of propofol. Intracranially recorded auditory cortical responses, including the AEP and high gamma activity, undergo adaptation to repeated stimuli (Eliades et al., 2014). This 10-minute baseline period was shown to be of sufficient duration to induce long-term adaptation, allowing this process to be dissociated from any additional effects produced by the propofol infusion. Following this 10-minute baseline period, an infusion of propofol was initiated at 50 μg/kg/min, and the infusion rate was increased every 10 minutes by 25 μg/kg/min. Propofol was delivered via an Alaris pump (Carefusion systems, Becton, Dickenson and Company, Franklin Lakes, NJ). No other sedative or anesthetic agents were administered. In all subjects except three, the propofol infusion lasted 50 minutes (56 minutes in subject L292, 62 minutes in subjects L314 and R316). The eventual induction of general anesthesia using these slowly escalated doses occurred at a more gradual rate compared to standard clinical practice and increased the average time spent in the operating room preceding the actual surgical procedure. There were no differences in perioperative

Author Manuscript Author Manuscript Author Manuscript Author Manuscript

management or the post-operative recovery of the research subjects compared to non-research epilepsy patients who underwent a more rapid anesthetic induction prior to electrode removal.

The infusions of propofol were administered by an anesthesiology resident or a certified registered nurse anesthetist and supervised by a faculty anesthesiologist. Standard respiratory, cardiac and hemodynamic monitors were always used. Supplemental oxygen was administered. Anesthesiologists could terminate the propofol infusion protocol at any time for the safety of the patients. The depth of sedation/anesthesia was continuously assessed using electroencephalographic spectral entropy monitoring (Viertiö-Oja et al., 2004; Bein, 2006) (E-ENTROPY module; Datex-Ohmeda Inc., Madison, WI). Surface electrodes for assessing anesthetic depth were applied to the forehead. Spectral entropy values have been shown to correlate with behavioral measures of propofol-induced sedation/anesthesia (Schmidt et al., 2004; Iannuzzi et al., 2005; Mahon et al., 2008) and to correlate with other electrophysiologic indices of depth of anesthesia with various anesthetics (Ellerkmann et al., 2004; Vakkuri et al., 2004; Vanluchene et al., 2004).

2.3. Recording

ECoG recordings were made from depth electrodes implanted in HG and subdural electrodes overlying STG. Electrode implantation, recording and ECoG data analysis have been previously described in detail (Howard et al., 1996, 2000; Reddy et al., 2010; Nourski et al., 2013; Nourski and Howard, 2015). All electrodes were placed solely on the basis of clinical requirements to identify seizure foci (Reddy et al., 2010; Nagahama et al., in review). The clinical purpose of electrodes placed in HG was to bracket the generator of the epileptic activity between superior and inferior aspects of the temporal lobe. Subdural electrode arrays overlying the STG and medial temporal lobe (e.g. parahippocampal gyris) further bracketed the suspected generator of epileptic activity along the medial-lateral dimension. Reviews of the outcomes of all patients implanted with depth electrodes in the HG within the last four years supports the strong clinical utility of these electrodes regarding the extent of surgical resections of diagnosed seizure foci (data available upon request).

Electrode arrays were manufactured by Ad-Tech Medical (Racine, WI). Depth electrode arrays (4–8 macro contacts, spaced 5–10 mm apart) targeting HG were stereotactically implanted in each subject along the anterolateral-to-posteromedial axis of the gyrus. Grid arrays consisted of platinum-iridium disc electrodes (2.3 mm exposed diameter, 5–10 mm inter-electrode distance) embedded in a silicon membrane. In all subjects, a subgaleal electrode was used as a reference. Collected ECoG data were amplified, filtered (0.7–800 Hz bandpass, 12 dB/octave rolloff), digitized at a sampling rate of 2034.5 Hz, and stored for subsequent offline analysis.

2.4. Data analysis

Response entropy (RE) is an index of the depth of anesthesia. It is an indicator of spectral entropy that includes both electroencephalogram and electromyogram components and is measured from electrodes placed on the forehead (Viertiö-Oja et al., 2004; Bein, 2006). RE was computed by E-ENTROPY module, details of analysis are provided in Viertiö-Oja et al.

Author Manuscript Author Manuscript Author Manuscript Author Manuscript

(2004). In brief, power spectrum of forehead-measured signals was calculated over a frequency range from 0.8 Hz to 47 Hz, with analysis time windows varying from 15.36 s to 1.92 s, respectively. The sum of these values was normalized so that the sum of the normalized power spectrum over the selected frequency region was equal to one. The Shannon function was applied to the each frequency component of the normalized power spectrum:

$$S=\frac{P\times\ln(\frac{1}{P})}{\ln(N)},$$

where S is the Shannon function, P is normalized spectral power, and N is the number of frequency components. The sum of these values, corresponding to entropy values, was transformed to a scale of integer values between 0 and 100 using a spline function (Viertiö-Oja et al. 2004). RE values computed by E-ENTROPY module were logged on a minute-by-minute basis over the time course of anesthetic induction with propofol.

The time course of anesthetic induction with propofol was characterized by fitting a four-parameter sigmoidal function to median RE values computed across the 10 subjects for the first 50 minutes of induction. Estimated brain concentrations of propofol as achieved by incrementally escalating infusion protocol were calculated for each subject (based on age, weight, gender, infusion rates and times) using software provided by Dr. Steven Shafer (Stanford University). This software is based on previously published pharmacokinetic and pharmacodynamic data (Schnider et al., 1998, 1999).

Reconstruction of the anatomical locations of the implanted electrodes and their mapping onto a standardized set of coordinates across subjects was performed using FreeSurfer image analysis suite and in-house software (see Nourski et al., 2014, for details). In brief, subjects underwent whole-brain high-resolution T1-weighted structural magnetic resonance imaging (MRI) scans (resolution 0.78×0.78 mm, slice thickness 1.0 mm) before electrode implantation. Two volumes were averaged to improve the signal-to-noise ratio of the MRI data sets and minimize the effects of movement artifact on image quality. After electrode implantation, subjects underwent MRI and thin-slice volumetric computerized tomography (CT) (resolution 0.51×0.51 mm, slice thickness 1.0 mm) scans. Contact locations of the HG depth electrodes and subdural grid electrodes were first extracted from post-implantation MRI and CT scans, respectively. These were then projected onto preoperative MRI scans using non-linear three-dimensional thin-plate spline morphing, aided by intraoperative photographs. For group analyses, these were projected into standard Montreal Neurological Institute (MNI) space (MNI305) using surface-based warping, with left hemisphere MNI x-axis coordinates (x_{MNI}) multiplied by (−1) to map them onto the right-hemisphere common space.

To allow for a straightforward interpretation of depth electrode locations in terms of their orientation along HG, the MNI coordinates were rotated along anatomical HG axis in the $x_{\mathrm{MNI}}y_{\mathrm{MNI}}$ plane, as previously described (Nourski et al., 2014). The coordinates in this plane were first centered by subtracting the grand mean location from each individual coordinate. Next, the best fit linear regression line was computed relating x_{MNI} to y_{MNI}. The

Author Manuscript Author Manuscript Author Manuscript Author Manuscript

corresponding angle of rotation, θ, was computed from the slope of that line. Finally, each set of coordinates was rotated by θ. This process resulted in the new x_θ coordinate which corresponded to the position along the long axis of HG with coordinate values increasing from posteromedial to anterolateral. HG sites were then divided into three equal-width groups according to their location along the gyrus.

Recording sites were included in analyses based on their anatomical location (i.e., implanted in the gray matter of the HG or overlying the lateral surface of the STG) as determined by the localization of each electrode in the pre-implantation MR for each subject individually, and not based on common MNI coordinates. Based on these criteria, a total of 84 HG recording sites (including 9 contacts in planum temporale) and 125 sites on lateral STG from the 10 subjects were examined. In three subjects (R330, R331 and R335), several depth electrode contacts were localized to planum temporale (2, 4 and 3 contacts, respectively). In subject R320, the depth electrode trajectory was localized to the gray matter of the anterior transverse sulcus. These contacts were included in analysis with sites in the crest of HG, as core auditory cortex extends onto the gray matter within the sulci surrounding HG (e.g. Rademacher et al., 2001; Da Costa et al., 2011).

Auditory cortical activity was measured and characterized as AEPs, FFRs, and high gamma event-related band power (ERBP). AEP waveforms were computed for each recording site on a minute-by-minute basis by time-domain averaging of up to 40 single-trial ECoG waveforms. Trials with any voltage deflections greater than five standard deviations from the mean calculated over the entire duration of the recording were excluded from subsequent AEP, FFR, and high gamma analyses. AEPs were characterized in terms of the latency of their early (within 40 ms after stimulus onset) peaks and the corresponding peak-to-peak amplitude.

Time-frequency analysis was carried out using a demodulation band transfer method (Kovach and Gander, 2016), a variant of the complex demodulation technique (Bingham et al., 1967), which in turn is closely related to the standard short-time Fourier transform (STFT). A more detailed description of this technique can be found in Kovach and Gander (2016). In brief, demodulation band transfer includes the following steps: (1) obtaining the discrete Fourier transform (DFT) of the entire signal; (2) segmenting the DFT into short overlapping intervals; (3) windowing each segment with a cosine window; (4) applying the inverse DFT to each segment. This procedure combines an analytic bandpass filter with downsampling and complex demodulation; in this respect, it is identical to the standard STFT, but because signal segmentation is carried out in the frequency domain rather than time, it avoids spectral leakage related to time-segmentation inherent to standard STFT. Additionally, this approach allows for a variable bandwidth, combining the advantages of bandpass quadrature filtering (i.e. Hilbert transform) with the computational efficiency of ordinary STFT. The resulting time-frequency distribution is used in the same way as with these alternative methods: the squared modulus of the signal at each moment reflects the power in the respective band around the given time.

In the present study, the demodulated band transfer technique was used to compute power within overlapping frequency windows of variable (1–20 Hz) bandwidth for theta (center

Author Manuscript Author Manuscript Author Manuscript Author Manuscript

frequencies 4–8 Hz, 1 Hz step), alpha (8–14 Hz, 2 Hz step), beta (14–30 Hz, 4 Hz step), gamma (30–70 Hz, 10 Hz step) and high gamma (70–150 Hz, 20 Hz step) ECoG bands. For each center frequency, the squared-modulus of the resulting complex signal was log-transformed, segmented into single trial epochs and, for each trial, normalized by subtracting the mean log power within a reference interval (100–200 ms before stimulus onset in each trial), and averaged over trials to obtain ERBP for each center frequency. FFR was estimated by calculating ERBP for a 50 Hz center frequency (equal to click rate) using a 5 Hz bandwidth parameter (Behroozmand et al., 2016). High gamma ERBP was calculated by averaging power envelopes for center frequencies between 70 and 150 Hz using a 20 Hz bandwidth parameter (i.e., in 20 Hz center frequency steps).

Changes in FFR and high gamma ERBP during anesthetic induction with propofol were evaluated for each recording site using the following approach. For both FFR and high gamma analysis, ERBP values were averaged within the interval of 0–500 ms after stimulus onset for each trial. ERBP during a pre-stimulus reference interval was computed for values within 100–200 ms before stimulus onset. Single-trial ERBP values computed over the 10th minute of the experiment (i.e., the minute immediately preceding induction onset) were compared to pre-stimulus reference values using paired one-tailed t-tests. Correction of p-values for multiple comparisons was done by controlling the false discovery rate (FDR) (Benjamini and Hochberg, 1995) using the linear step-up procedure, as implemented in MATLAB Version 7.14 Bioinformatics Toolbox. Sites that exhibited a significant ($p < 0.05$) response were then evaluated for response changes during the infusion of propofol. Linear regression between estimated brain concentration of propofol (μg/ml) and response magnitude (dB ERBP) was used to establish the direction of changes. For a given site, significant ($p < 0.05$) positive Spearman's rank correlation coefficient (ρ) values were interpreted as indicative of an increase in the magnitude of response with the concentration of propofol. Sites characterized by negative or non-significant positive ρ-values were evaluated for the rate of response decay during induction by fitting a decaying exponential to the propofol concentration vs. response magnitude data. Decay constant (κ) values associated with the fits were used to characterize the sensitivity of individual sites to propofol induction.

3. Results

3.1. Time course of propofol induction

In all cases, the protocol for the infusion of propofol was completed without the need for early termination or any apparent complications. Changes in the level of consciousness of each subject as measured by response entropy (RE) were monitored during the administration of propofol. Figure 1A shows the time course of the infusion and concurrent changes in RE. RE values between 40 and 60 (i.e., recommended range for adequate anesthesia; Bein, 2006) were typically observed at approximately 20 minutes after induction onset, corresponding to a propofol infusion rate of 100 μg/kg/min. While in most subjects RE was stable during the 10-minute interval that preceded induction, it decreased in three subjects (R263, R320 and R331) likely reflecting the patient becoming drowsy that was unrelated to drug infusion. On average, the time course of RE changes during induction was

Author Manuscript Author Manuscript Author Manuscript Author Manuscript

characterized by a sigmoidal function, though RE values at any given point in time varied considerably across subjects (Fig. 1B). This variability in part reflects transient arousal likely related to sensory stimulation during preoperative procedures. Due to this variability in RE over time, propofol brain concentrations were estimated on a minute-by-minute basis based on models of propofol pharmacokinetics and pharmacodynamics (Schnider et al., 1998, 1999) (Fig. 1C). Estimated brain concentrations of propofol were used as the independent variable in subsequent analyses in this study.

3.2. Auditory cortical responses to click train stimuli before induction

Click trains with a repetition rate of 50 Hz elicited stereotypical response profiles in the AEP, FFR, and high gamma ERBP in HG and on lateral STG (Fig. 2). Electrode coverage of auditory cortex in a representative subject is depicted in Figure 2A. The most posteromedial portion of HG (site ‘a’) was characterized by short-latency large-amplitude AEPs, with responses elicited by both the onset and the offset of the 500 ms stimulus (Fig. 2B). A 50 Hz periodicity representing the FFR was superimposed upon the AEP waveform. This sustained FFR was evident in the time-frequency plane as an increase in ERBP at the driving frequency (50 Hz). Finally, there was an increase in high gamma power elicited by the stimulus. Together, these patterns represent a neural signature of posteromedial HG (Nourski and Brugge, 2011).

A marked change occurred along HG when recording from anterolateral HG (site ‘b’). Here, responses were characterized by long latency, broad AEP deflections of lower amplitude, absence of the FFR, and minimal changes in high gamma power induced by the stimulus.

In contrast to the orderly change in the physiological responses elicited by the click train stimuli in HG, responses along the lateral STG were characterized by considerable site-to-site variability. Some sites (e.g. ‘c’) exhibited AEPs intermediate in onset latency between posteromedial and anterolateral HG, and featured FFRs and high gamma responses. Other sites on STG, such as ‘d’, were weakly activated by this stimulus, and, in this example, featured a low-amplitude off response.

These activity profiles are consistent with previous reports of responses recorded from HG and STG to simple non-speech stimuli such as click trains and pure tones (Brugge et al., 2009; Nourski et al., 2013; Nourski et al., 2014). This validates their use as benchmark measures in the study of auditory cortical modulation by propofol anesthesia.

3.3. Effects of propofol: HG

Propofol infusion modulated AEP, FFR, and high gamma responses in posteromedial HG in two different ways (Fig. 3). A schematic of the experimental paradigm used to assess these changes is shown in Figure 3A. AEPs, FFR, and high gamma ERBP were computed on a minute-by-minute basis. Locations of two exemplary sites in posteromedial HG are depicted in Figure 3B. The time course of changes in AEP, FFR, and high gamma activity is presented in Figure 3C. Here, each color plot represents a series of one-minute response averages stacked from top to bottom according to time relative to induction onset.

Author Manuscript Author Manuscript Author Manuscript Author Manuscript

In the most posteromedial portion of the gyrus, exemplified by site ‘a’, short-latency AEPs persisted throughout induction, albeit with increases in onset and peak latencies. Notably, the FFR at 50 Hz increased in power as propofol brain concentration increased. This increase occurred regardless of whether the FFR was measured as ERBP (i.e. baseline-normalized) or as absolute ECoG power at 50 Hz (data not shown). High gamma activity elicited by the onset of the stimulus also persisted throughout induction, although the response to stimulus offset was attenuated. Different patterns were observed at recording sites located at slightly more intermediate positions in the gyrus (site ‘b’). Here, both the AEP and the FFR were attenuated in parallel with increases in propofol concentration. As for many sites in intermediate portions of HG, there was minimal high gamma ERBP even prior to induction onset.

Due to a considerable variability in AEP morphology across auditory cortical regions (see Fig. 2), quantitative analyses were unsuitable for assessing AEPs. Instead, we focused on the early peaks of the AEP waveform that were reliably observed in the posteromedial HG. Persistence of early AEP deflections during induction was a consistent finding across subjects in the most posteromedial HG locations, as exemplified by site ‘a’ in Figure 4A. Color maps represent the polarity and amplitude of the first 200 ms of the AEP waveforms. Waveforms immediately preceding induction are plotted above the color maps. Initial activity peaked at around 18 and 32 ms. The designation *P*/*N* refers to the fact that polarity depends upon the laminar location of the recording electrode with respect to the cellular generators, and thus the peaks were labeled without any assumption regarding their manifestations at the scalp.

The earliest activity (P/N_{18}) persisted throughout induction with a minimal increase in peak latency (Fig. 4B, red symbols). The following deflection at 32 ms also persisted throughout induction, although its latency increase was proportionately greater than that of the earlier peaks (Fig. 4B, blue symbols). There was a trend for an increase in peak-to-peak amplitude at early points in the induction, followed by either a plateau or a decrease (Fig. 4B, black symbols). The later positive (i.e. downward) deflection in the AEP that initially peaked at around 60 ms increased in latency and decayed in amplitude at high propofol concentrations (see Fig. 4A, site ‘a’). The width of the P/N_{32} component increased in parallel with attenuation of the following positivity. This finding indicates that it is inaccurate to ascribe each peak to a discrete generator. Instead, these waveforms represent a complex sum of multiple synaptic events. In this case, later synaptic activity is more sensitive to propofol anesthesia, allowing for the less susceptible earlier components to broaden.

Pronounced changes in the AEP occurred at slightly more intermediate locations along HG (Fig. 4A, site ‘b’). In this example, recording site ‘b’ was only 10 mm away from site ‘a’, and reconstructions of electrode locations indicated that both were located in infragranular layers of auditory cortex gray matter (data available upon request). The overall morphology of the AEP on site ‘b’ was different from that on site ‘a’; amplitudes were smaller and the early components were more variable and more susceptible to attenuation over the course of propofol infusion. In both examples (‘a’ and ‘b’), portions of the AEP waveform that represented later synaptic activity dissipated prior to shorter-latency AEP components.

Author Manuscript Author Manuscript Author Manuscript Author Manuscript

Changes in FFR with increasing concentrations of propofol were location-dependent along HG (Fig. 5). In the majority of subjects, the most posteromedial sites were characterized by an increase in FFR. In contrast, intermediate locations showed a decrease in FFR, while in anterolateral portions the FFR was absent. These three patterns are illustrated in Figure 5A. In this subject (L258), the two most posteromedial sites ('a' and 'b') showed significant increases in FFR power during induction. The more intermediate site ('c') showed a progressive decrease in the FFR that could be described by an exponential decay function. The exponential decay constant, κ, refers to the propofol concentration at which response magnitude dropped to approximately 37% of its initial value. The most anterolateral site ('d') did not exhibit an FFR. These three FFR patterns were consistent across subjects, and demonstrated anatomical clustering along the gyrus (Fig. 5B).

This clustering was demonstrated by plotting HG electrode sites from all subjects in standard MNI coordinate space, and color-coding them according to the observed pattern of changes in FFR (Fig. 5B, bottom panel). Increases in FFR were restricted to the most posteromedial tip of HG. Responses within the middle portion of the gyrus decayed during propofol induction. The anterolateral portion of HG did not phase-lock to the click train repetition rate regardless of the subjects' state of arousal. Sites characterized by the longest decay constants ($\kappa \geq 4$ μg/ml) were intermixed with those exhibiting FFR increases. There was a negative correlation between location along the gyrus and the decay constant in HG ($\rho = -0.690$, $p < 0.001$).

Changes in high gamma ERBP were less sensitive markers for delineating subregions along HG. As a rule, sustained high gamma activity elicited by the 50 Hz click train stimulus was restricted to the posteromedial third of the gyrus and decayed during induction (Fig. 6). The presence of high gamma activity at individual sites correlated with sites that showed increases in FFR strength during propofol induction (Fisher's exact test $p < 0.001$). To investigate whether restriction of high gamma activity to the posteromedial third of HG was based on examining sustained activity throughout the entire 500 ms peristimulus interval, we measured high gamma within the first 200 and 250 ms following the stimulus onset. No significant differences were identified in the number or distribution of sites that exhibited significant high gamma responses.

3.4. Effects of propofol: STG

Whereas a simple non-speech sound such as 50 Hz click train is an adequate stimulus to generate various response types in HG, it is suboptimal for assessment of regional differentiation in putative parabelt regions of the auditory cortex located on the lateral STG (Chevillet et al., 2011; Nourski et al., 2014). While AEPs were present on the lateral STG (see Fig. 2B), only 13 sites out of 125 exhibited significant FFR, and only two sites showed sustained high gamma responses. These responses were scattered across the extent of STG without any clear clustering to specific loci. For these reasons, quantitative analyses of FFR and high gamma in this study were limited to activity in HG, leaving open future assessments of STG with more complex stimulus paradigms.

Author Manuscript Author Manuscript Author Manuscript Author Manuscript

3.5. Relationship between effects of propofol and basic response properties of HG

Changes in effects of propofol on cortical activity along HG were summarized by dividing HG into equal-width regions of interest. These divisions were based on the relative position of each site along the axis of the gyrus (posteromedial, middle and anterolateral), as described in Methods. Phase-locked activity was least attenuated by propofol in the posteromedial third of HG, exhibiting either increases or decreasing only at the highest propofol doses tested (Fig. 7A). There was a progressive decrease in the presence of FFRs in the middle and anterolateral portions of the gyrus. When present, FFRs were highly susceptible to propofol as assessed by decay constants. Finally, sustained high gamma activity elicited by 50 Hz click trains was predominantly present on sites within the posterior third of HG and typically decreased during induction (Fig. 7B).

During the period that subjects were implanted with intracranial electrodes for chronic monitoring, brain responses were recorded in response to a wide range of sounds presented in multiple experimental paradigms. Fundamental to all recordings in auditory cortex were a series of sound presentations designed to help define basic spectral and temporal response properties at different auditory cortical sites. These included experimental paradigms that examined the sensitivity and specificity of recording sites to pure tones of different frequencies.

Previous studies in non-human primates have shown FFRs are maximal within high best frequency regions of primary auditory cortex (Steinschneider et al., 1998; Fishman et al., 2000; O'Connell et al., 2015), reflecting phase locking capabilities that emerge at the level of the auditory nerve (Cariani and Delgutte, 1996). Several fMRI studies in humans have suggested that the most posteromedial portion of HG is most sensitive to high frequency tones (Formisano et al., 2003; Moerel et al., 2013; De Martino et al., 2015). Thus, we examined whether the persistence of the FFR under anesthesia and presence of sustained high gamma ERBP during the baseline period in the posteromedial portion of HG were a function of pure tone sensitivity. High gamma ERBP was measured in response to six pure tone stimuli presented at moderate intensities ranging from 0.25 to 8 kHz in octave intervals (Fig. S1). Recording sites along HG, including its most posteromedial portion, were broadly tuned but had maximal responses at 0.5–2 kHz.

Relationship between best frequency (BF) and the magnitude of FFR or high gamma responses to click trains prior to propofol induction was examined in the sample of 50 HG sites that could be characterized by a BF (see Supplementary Methods and Fig. S1). BFs ranged from 0.25 to 8 kHz, with the majority of sites characterized by BFs of 0.5 or 1 kHz. The comparison between tonotopy and responses to click trains was carried out using linear regression analysis and ANOVA. Linear regression failed to reveal a significant relationship between BF and FFR ($r^2 = 0.0143$; $p = 0.408$) and between BF and high gamma ($r^2 = 0.0638$ $p = 0.0767$). Likewise, ANOVA failed to reveal a significant relationship between tonotopy and response to click trains (for BF Vs. FFR, $F(5,44) = 0.36$, $p = 0.876$; for BF Vs. high gamma, $F(5,44) = 0.97$, $p = 0.449$). Thus, contrary to our prediction, sites within posteromedial HG that displayed FFRs did not reliably exhibit a preference for high frequency tones.

Author Manuscript Author Manuscript Author Manuscript Author Manuscript

In addition to testing spectral sensitivity with pure tone stimuli, high gamma onset latencies were measured using brief 100 Hz click trains, as described previously (Nourski et al., 2014). These stimuli elicit more robust high gamma responses compared to 50 Hz click trains, albeit at the expense of the FFR (Brugge et al., 2009; Nourski et al., 2013). The most posteromedial aspect of HG exhibited the shortest high gamma onset latencies (Fig. S2). The response latencies progressively increased along the gyrus towards its anterolateral aspect.

4. Discussion

4.1. Summary of findings

The present study utilized a novel protocol for an incrementally titrated infusion of propofol that allowed for a gradual increase in its brain concentration with the induction of anesthesia. Our main finding was the persistence of auditory responses to acoustic transients (500 ms 50 Hz click trains) in the posteromedial third of HG, with preservation of the earliest AEP deflections and an increase in FFRs, along with a parallel decrease in sustained and non phase-locked high gamma ERBP. In contrast, FFRs within the middle third of HG typically decreased over the course of induction, while sites in the anterolateral HG and on STG were either non-responsive, or were characterized by rapidly decaying FFRs.

4.2. Interpretation of AEP, FFR and high gamma results

Click train stimuli elicited AEP waveform complexes associated with both stimulus onset and offset (see Fig. 2, 3). The latter off-responses were particularly prominent in the posteromedial portion of HG. This finding conforms to previously described intracranial response patterns elicited by click trains (Brugge et al., 2009; Nourski & Brugge, 2011; Nourski et al., 2013). Typically, off-responses become progressively more prominent as click trains increase in repetition rate, mirroring response profiles seen in field potentials and multiunit activity recorded in awake macaques (Steinschneider et al., 1998). In the present study, AEPs elicited by the stimulus offset were attenuated or diminished over the course of induction, with a time course different from attenuation of AEPs elicited by the stimulus onset. Future work will have to be performed in order to more fully characterize mechanisms underlying the differential effects of anesthesia on responses elicited by stimulus onsets and offsets.

The earliest components of the AEP response to stimulus onset reflect synaptic activity derived from direct thalamocortical inputs generated by the lemniscal pathway and the earliest intracortical synaptic events (e.g. Steinschneider et al., 1992). The present results are consistent with a model in which anesthetic concentrations of propofol have limited effect on feedforward thalamocortical sensory signals. What is disrupted, however, is the interlaminar processing of auditory signals within posteromedial HG and downstream activation of non-core auditory areas. This disruption of interlaminar processing occurs in a stepwise manner, with later AEP components being affected at lower brain propofol concentrations than earlier components (Fig. 4; cf. Howard et al., 2000). Disruption of these later events by propofol reveals prolonged early synaptic events, which may be truncated by subsequent activity in the non-anesthetized state. This process is exemplified by changes in the AEP as shown in Figure 4A (site ‘a’), where the duration and peak latency of the early

Author Manuscript Author Manuscript Author Manuscript Author Manuscript

P/N_{32} increased as the following waveform deflection was suppressed. Similar results are seen at more intermediate locations on HG (e.g. Figure 4A, site 'b'). These findings represent a fundamental property of AEPs, wherein waveforms are derived from a complex summation of current sources and sinks weighted by their strength, synchrony, dipole orientation and distance from the recording site (Steinschneider et al., 1994; Eggermont and Ponton, 2002). Thus, propofol (and perhaps other anesthetic agents) provide a method to isolate specific stages in both inter-regional and interlaminar cortical processing.

The FFR in the posterior third of HG increased in its relative magnitude over the course of propofol induction. In a manner similar to that seen with early AEP components, the FFR is likely dominated by synaptic events derived directly from thalamocortical inputs. Two mechanisms may contribute to this observed increase. First, thalamocortical synapses exhibit high release probability and short-term depression under awake conditions (Chung et al., 2002). Propofol anesthesia may reduce neurotransmitter release probability and thereby introduce short term facilitation, leading to the increase in sustained FFR (Ratnakumari and Hemmings, 1997; Yang et al., 2015). Our results parallel the findings of Sullivan et al. (2015) who described an increase in auditory steady state responses in the rat auditory cortex treated with MK-801, an NMDA receptor antagonist. Second, current findings suggest that phase locking in core auditory cortex may be unmasked by the suppression of simultaneous non-phase locked synaptic events initiated from other cortical and subcortical regions that project to core cortex. Thus, we propose that propofol suppresses this top-down processing, unmasking the temporally precise FFR from MGv inputs to core auditory cortex.

In contrast, more intermediate areas in HG showed a decrease in FFR magnitude with increasing concentration of propofol during anesthetic induction. Synaptic responses in this part of HG may be depressed to a greater degree, such that facilitation is not manifested and residual Ca^{2+} in synaptic terminals can no longer produce larger responses throughout the duration of the train. Additionally, this decrease would not be expected if a major source of inputs were the same as that to the more posteromedial sites. There are several possible mechanisms that can account for this decrease. First, responses in intermediate areas may reflect phase-locked inputs from regions of thalamus that are more susceptible to propofol. Second, the sensitivity of cortical GABA-ergic circuits to propofol may be greater in intermediate areas compared to posteromedial areas, suppressing the FFR in the latter region directly. Third, the FFR in intermediate regions may arise in part due to feedforward cortico-cortical projections from the most posteromedial portion of HG. Propofol suppresses high gamma activity in the posteromedial portion of HG and thus would disrupt this feedforward cortico-cortical signal.

Sustained high gamma activity, a surrogate for unit activity, either uniformly decreased with induction of propofol anesthesia, or was not present at the beginning of induction. Only one site out of 87, located in the most posteromedial portion of HG, exhibited an increase in high gamma ERBP magnitude with propofol level. The absence of sustained high gamma on the more anterolateral HG regions and on lateral STG at the beginning of induction should not be viewed as a sign that the 50 Hz click train stimulus did not activate these regions. In many cases, there has been sustained high gamma at the beginning of the experimental block, which habituated by the time propofol infusion was initiated (cf. Eliades et al., 2014).

Author Manuscript Author Manuscript Author Manuscript Author Manuscript

Further, we used a conservative metric to establish the significance of high gamma responses by averaging power over the entire 500 ms peristimulus interval referenced to the pre-stimulus baseline. Transient increases in high gamma ERBP elicited by stimulus onset could be counterbalanced by the absence of power throughout the rest of the peristimulus interval when compared for statistical significance with pre-stimulus values.

The cortical areas within posteromedial HG, where high gamma responses were observed prior to and throughout the period of anesthesia induction, also demonstrated short-latency AEPs and FFRs that were resistant to propofol. Within this region of HG the FFRs increased in relative magnitude during induction. These effects are likely dependent on the presence of strong feedforward connectivity with the MGN that is diminished or absent at more lateral locations along HG. Thus, the posteromedial two thirds of HG were not uniform in their basic response properties and could be parcellated into at least two subdivisions.

Non-speech stimuli, such as click trains used in the present study, may not be particularly salient stimuli for these auditory areas, especially when presented in a passive listening paradigm (Nourski et al., 2014, 2015). In future experiments, more diverse sets of complex stimuli will need to be used to better characterize and refine the boundaries of these regions.

4.3. Relationship with models of human auditory cortex organization

It is difficult to completely reconcile current observations with many existing models of human auditory cortex organization, which, in most general terms, describe posteromedial two thirds of HG as core auditory cortex. We posit several possible explanations for the current findings. First, the two functional subdivisions within posteromedial HG observed in the present study might be confined to primary auditory cortex. If this is the case, it might be expected that the most posteromedial portion of HG would be characterized by high best frequencies. It would explain why the FFR is most prominent in the most posteromedial portion of HG, as multiple studies have shown that phase locking to repetitive acoustic transients is most prominent in high-frequency portions of A1 (e.g. Steinschneider et al., 1998; Fishman et al., 2000). A number of human fMRI studies suggest a tonotopic organization compatible with this interpretation (e.g. Formisano et al., 2003; Talavage et al., 2004). However, we did not observe this relationship between tonotopy and phase locking in our relatively limited subject sample (see Fig. S1).

More recent work suggests a more refined organization wherein the high-low-high frequency best gradients within core auditory cortex follow a V-shaped configuration (reviewed in Baumann et al., 2013; Moerel et al., 2014; Saenz and Langers, 2015). This configuration posits that a large portion of the crest of HG is characterized by preference for relatively low frequencies. Our spectral sensitivity results are in general agreement with this configuration, but are not concordant with enhancement of FFRs to repetitive acoustic transients in high best frequency regions, as described in the monkey (Steinschneider et al., 1998; Fishman et al., 2000). It must be acknowledged that our assessment of spectral sensitivity was made with suprathreshold stimuli, where even regions of high best frequencies would be expected to be strongly responsive to lower frequencies (tail of the tuning curve; Kiang and Moxon, 1972; Sutter, 2000). Further, our assessments were made using high gamma ERBP as measured from low-impedance cylindrical electrode contacts.

Author Manuscript Author Manuscript Author Manuscript Author Manuscript

Greater specificity has been shown with microelectrode recordings and those of single units from human auditory cortex (Howard et al., 1996; Bitterman et al., 2008; Jenison et al., 2015).

Human primary auditory cortex is characterized by intraareal compartmentalization, which has been visualized as differences in cytochrome oxidase and acetylcholinesterase staining in post-mortem brains (Clarke and Rivier, 1998). Such a compartmentalization could potentially contribute to differences in the sensitivity of click train-evoked responses to propofol. Further studies, likely involving well-controlled pharmacological manipulations in experimental animals, will be required to test the hypothesis that the observed electrophysiological findings represent intraareal differences within primary auditory cortex.

Another possibility is that these two subdivisions within posteromedial HG represent an area boundary within core auditory cortex. A number of anatomical studies have argued for a similar result. While we find this a promising interpretation, aspects of these proposed boundaries do not strictly conform to the current observations. In their classic study, Galaburda and Sanides (1980) described a double koniocortical core region, comprised of medial and lateral areas (KAm and KAlt, respectively). However, KAm and KAlt are envisioned to run in parallel along the axis of HG, whereas our results suggest a functional boundary orthogonal to this axis.

Multiple other organizational schemes divide HG into three regions along its long axis based on cytoarchitectonic criteria (von Economo and Koskinas, 1925; Beck, 1928; von Economo & Horn, 1930; Morosan et al., 2001; reviewed in Hackett, 2007, 2015). These parcellation schemes are consistent with the distribution of FFR changes along HG reported in the present study (see Fig. 8). In the model proposed by Morosan et al. (2001), the putative primary auditory cortex is subdivided into three areas, Te1.1, Te1.0 and Te1.2, running from posteromedial to anterolateral HG. While Morosan et al. (2001) interpreted area Te1.0 as the quintessential koniocortex, other studies have shown that the densest myelination, a typical feature of primary sensory cortex and its thalamocortical input in all three major modalities (auditory, visual and somatosensory), occurs in the most posteromedial portion of HG (Hackett et al., 1998, 2001; De Martino et al., 2015), more likely corresponding to area Te1.1 of Morosan et al. (2001). This in turn would explain why the shortest-latency AEPs and the FFR would be resistant to propofol anesthesia, as they reflect this feedforward thalamocortical connectivity.

Complementary auditory cortex parcellation studies based on neurochemical criteria (e.g. Chiry et al., 2003; Sacco et al., 2009) may have direct bearing on the regional differences in responses to click train stimuli and their sensitivity to propofol anesthesia. In a study of Chiry et al. (2003), immunohistochemical assessment of calcium-binding protein distribution along HG revealed more prominent staining for parvalbumin and calretinin in the middle third of HG compared to its most medial portion. This distribution is consistent with the cytoarchitectonic-based parcellation scheme of Morosan et al. (2001) (areas Te1.1 and Te1.0) as well as with the present electrophysiology findings. $GABA_A$ (ionotropic) and $GABA_B$ (metabotropic) receptor distributions along HG (Sacco et al., 2009) parallel cytoarchitectonic parcellations (von Economo and Koskinas, 1925; Morosan et al., 2001) as

Author Manuscript Author Manuscript Author Manuscript Author Manuscript

well as some of the current results. It is difficult to relate the patterns of GABA receptor distribution reported by Sacco et al (2009) to our current findings, as the most medial portion of HG, i.e. von Economo's area TD, was not examined in that study. Overall, how the differences in neurochemical profiles across auditory cortical areas lead to an increase, a decrease or absence of phase-locking in the medial, middle and lateral third of HG, respectively, is unknown and will most likely require neurochemical manipulations in experimental animals to clarify the mechanisms at play.

Two additional schemes of human auditory cortical organization are based on models of functional neuroanatomy developed in non-human primates (e.g. Rauschecker et al., 1995; Hackett et al., 1998; Kaas and Hackett, 2005). The first scheme divides the posteromedial two thirds of HG into human homologs of monkey core areas A1 and R (Moerel et al., 2014; Brewer and Barton, 2016). Both areas A1 and R receive principal thalamic input from the ventral division (MGv) of MGN (de la Mothe et al., 2006) and both are characterized by similar "koniocortical" cytoarchitecture (Hackett et al., 2001). The principal differences are based on a functional reversal of tonotopy (Merzenich and Brugge, 1973; Morel et al., 1993), an organization we may not have been able to adequately assess, and myelination, which is denser in A1 compared to R (Hackett et al., 1998). High-resolution MRI mapping of superior temporal plane myeloarchitecture using T1/T2 contrasts (Wasserthal et al., 2014; De Martino et al., 2015) in the same cohort of subjects can be informative for testing the hypothesis that the differential sensitivity of posteromedial two thirds of HG to propofol reflects a boundary between the human homologs of areas A1 and R.

An alternative scheme is that the region within the posteromedial third of HG corresponds to the human homolog of caudomedial belt area CM. This suggestion is compatible with some neuroanatomical models of human auditory cortex, which envision the most posteromedial portion of HG to be a belt area (see Hackett et al., 2001; Hackett, 2007, for reviews). Area CM is unusual among the eight auditory belt areas described in non-human primates in that it exhibits remarkably short onset response latencies, being as fast or even faster than A1 (Kajikawa et al., 2005; Camalier et al., 2012). This is consistent with our observations (see Fig. S2). Area CM receives thalamic projections mainly from the anterodorsal division of MGN (e.g. de la Mothe et al., 2006; Bartlett and Wang, 2011). Like MGv, anterodorsal MGN is a specific thalamic nucleus that appears to be part of the lemniscal auditory pathway (Hackett et al., 2007). Functionally, area CM in the monkey is principally involved in sound localization as part of the dorsal stream of auditory cortical processing (Recanzone et al., 2000; Recanzone and Cohen, 2010). Future studies could thus test the functional homology between area CM and the most posteromedial portion of HG in humans. As area CM is envisioned to be part of the posterodorsal auditory processing pathway (the "where" pathway), neurons there exhibit a greater sensitivity to stimulus location in space compared to neurons in A1 (Recanzone et al., 2000). Thus, testing sensitivity of the posterior-most portion of HG to sound location using fMRI in the same subjects (or using ECoG in future intracranial studies) may help address the possibility of its potential identity as the human homolog of area CM.

Author Manuscript Author Manuscript Author Manuscript Author Manuscript

4.4. Relevance for understanding the neural basis of sensory awareness

This study represents a first step in our using anesthetic agents as a research tool to understand how sensory activation of the cortical hierarchy reflects sensory awareness. Current findings are compatible with other studies investigating the effects of propofol anesthesia on cortical processing of external stimuli. Middle latency components of the scalp-recorded AEP and N_{20} of the somatosensory evoked potential (SSEP) persist throughout induction of anesthesia with propofol (e.g. Huotari et al., 2004; Shwilden et al., 2005). Earliest components of the middle latency AEP reflect initial stages of primary auditory cortical activation by MGv (e.g. Müller-Preuss and Mitzdorf, 1984; Steinschneider et al., 1992) and are concordant with the earliest AEP deflections measured in the posteromedial HG (e.g. P/N_{18} and P/N_{30}). Preservation of the scalp-recorded components is thus consistent with the preservation of P/N_{18} and P/N_{30} in the present study. The N_{20} component of the SSEP, the earliest activation of primary somatosensory cortex within Brodmann area 3b (Arezzo et al., 1981), is also preserved under propofol anesthesia (Huotari et al., 2004; Shwilden et al., 2005), as are the earliest components of the visual evoked potential (Schroeder et al., 1991).

Early evoked components are also preserved during normal physiologic loss of consciousness as seen in NREM sleep, and in pathologic loss of consciousness as seen in minimally responsive and the chronic vegetative state (Portas et al., 2000; Dang-Vu et al., 2011; Faugeras et al., 2012; Strauss et al., 2015). Thus, as a general rule, initial cortical processing within primary sensory areas is relatively resistant to the effects of loss of consciousness. In contrast, later activity dominated by activation in higher-order sensory areas is more sensitive to general anesthetics and to loss of consciousness under physiologic and pathologic states (Bekinschtein et al., 2009; Mashour, 2014; Raz et al., 2014; Strauss et al., 2015). Suppression of higher order sensory areas was exemplified by the attenuation of the AEP and FFR in all areas outside the most posteromedial portion of HG and its immediate surrounds. Future experiments capitalizing on upon regional differences in the sensitivity to anesthesia as well as examining regional differences in responses to more complex stimuli such as speech may provide further insights into the link between sensory processing and sensory awareness (Bastuji et al., 2002; Friston, 2005) and have significant ramifications for rehabilitation programs in patients in minimally responsive or chronic vegetative states.

Supplementary Material

Refer to Web version on PubMed Central for supplementary material.

Acknowledgments

We thank John Brugge, Haiming Chen, Phillip Gander, Bradley Hindman, Christopher Kovach, Richard Reale and Xiayi Wang (The University of Iowa), Bryan Krause (University of Wisconsin – Madison), and Steven Shafer (Stanford University), for help with data acquisition and analysis. This study was supported by grants NIH R01-DC04290, NIH R01-GM109086, NIH UL1-RR024979, NSF CRCNS-IIS-1515678 and the Hoover Fund.

Author Manuscript Author Manuscript Author Manuscript Author Manuscript

Abbreviations

AEP	averaged evoked potential
BF	best frequency
CT	computerized tomography
ECoG	electrocorticography
ERBP	event-related band power
FDR	false discovery rate
FFR	frequency-following response
fMRI	functional magnetic resonance imaging
HG	Heschl's gyrus
HL	hearing level
MGN	medial geniculate nucleus
MGv	ventral division of medial geniculate nucleus
MNI	Montreal Neurological Institute
MRI	magnetic resonance imaging
MMN	mismatch negativity
RE	response entropy
SSEP	somatosensory evoked potential
STG	superior temporal gyrus

References

Amzica F, Massimini M, Manfridi A. Spatial buffering during slow and paroxysmal sleep oscillations in cortical networks of glial cells in vivo. J Neurosci. 2002; 22:1042–1053. [PubMed: 11826133]

Arezzo JC, Vaughan HG Jr, Legatt AD. Topography and intracranial sources of somatosensory evoked potentials in the monkey. II. Cortical components. Electroencephalogr Clin Neurophysiol. 1981; 51:1–18. [PubMed: 6161773]

Bai D, Pennefather PS, MacDonald JF, Orser BA. The general anesthetic propofol slows deactivation and desensitization of GABA(A) receptors. J Neurosci. 1999; 19:10635–10646. [PubMed: 10594047]

Bartlett EL, Wang X. Correlation of neural response properties with auditory thalamus subdivisions in the awake marmoset. J Neurophysiol. 2011; 105:2647–2667. [PubMed: 21411564]

Bastuji H, Perrin F, Garcia-Larrea L. Semantic analysis of auditory input during sleep: studies with event related potentials. Int J Psychophysiol. 2002; 46:243–255. [PubMed: 12445951]

Baumann S, Petkov CI, Griffiths TD. A unified framework for the organization of the primate auditory cortex. Front Syst Neurosci. 2013; 7:11. [PubMed: 23641203]

Author Manuscript Author Manuscript Author Manuscript Author Manuscript

Beck E. Die myeloarchitektonische Felderung es in der Sylvischen Furche gelegenen Teiles des menschlichen Schlafenlappens. J Psych Neurol. 1928; 36:1–21.

Behroozmand R, Oya H, Nourski KV, Kawasaki H, Larson CR, Brugge JF, Howard MA 3rd, Greenlee JD. Neural Correlates of Vocal Production and Motor Control in Human Heschl's Gyrus. J Neurosci. 2016; 36:2302–2315. [PubMed: 26888939]

Bein B. Entropy. Best Pract Res Clin Anaesthesiol. 2006; 20:101–109. [PubMed: 16634417]

Bekinschtein TA, Dehaene S, Rohaut B, Tadel F, Cohen L, Naccache L. Neural signature of the conscious processing of auditory regularities. Proc Natl Acad Sci U S A. 2009; 106:1672–1677. [PubMed: 19164526]

Benjamini Y, Hochberg Y. Controlling the false discovery rate: a practical and powerful approach to multiple testing. J R Stat Soc B. 1995; 57:289–300.

Bingham C, Godfrey MD, Tukey JW. Modern techniques of power spectrum estimation. IEEE Trans Audio Electroacoustics. 1967; 15:56–66.

Bitterman Y, Mukamel R, Malach R, Fried I, Nelken I. Ultra-fine frequency tuning revealed in single neurons of human auditory cortex. Nature. 2008; 451:197–201. [PubMed: 18185589]

Boly M, Moran R, Murphy M, Boveroux P, Bruno MA, Noirhomme Q, Ledoux D, Bonhomme V, Brichant JF, Tononi G, Laureys S, Friston K. Connectivity changes underlying spectral EEG changes during propofol-induced loss of consciousness. J Neurosci. 2012; 32:7082–7090. [PubMed: 22593076]

Brewer AA, Barton B. Maps of the Auditory Cortex. Annu Rev Neurosci. 2016; 39:385–407. [PubMed: 27145914]

Brugge, JF., Howard, MA. Hearing. In: Ramachandran, VS., editor. Encyclopedia of the Human Brain. Academic Press; New York: 2002. p. 429-448.

Brugge JF, Volkov IO, Oya H, Kawasaki H, Reale RA, Fenoy A, Steinschneider M, Howard MA III. Functional localization of auditory cortical fields of human: click-train stimulation. Hear Res. 2008; 238:12–24. [PubMed: 18207680]

Brugge JF, Nourski KV, Oya H, Reale RA, Kawasaki H, Steinschneider M, Howard MA. Coding of repetitive transients by auditory cortex on Heschl's gyrus. J Neurophysiol. 2009; 102:2358–2374. [PubMed: 19675285]

Camalier CR, D'Angelo WR, Sterbing-D'Angelo SJ, de la Mothe LA, Hackett TA. Neural latencies across auditory cortex of macaque support a dorsal stream supramodal timing advantage in primates. Proc Natl Acad Sci U S A. 2012; 109:18168–18173. [PubMed: 23074251]

Cariani PA, Delgutte B. Neural correlates of the pitch of complex tones. II. Pitch shift, pitch ambiguity, phase invariance, pitch circularity, rate pitch, and the dominance region for pitch. J Neurophysiol. 1996; 76:1717–1734. [PubMed: 8890287]

Chevillet M, Riesenhuber M, Rauschecker JP. Functional correlates of the anterolateral processing hierarchy in human auditory cortex. J Neurosci. 2011; 31:9345–9352. [PubMed: 21697384]

Chiry O, Tardif E, Magistretti PJ, Clarke S. Patterns of calcium-binding proteins support parallel and hierarchical organization of human auditory areas. Eur J Neurosci. 2003; 17:397–410. [PubMed: 12542677]

Chung S, Li X, Nelson SB. Short-term depression at thalamocortical synapses contributes to rapid adaptation of cortical sensory responses in vivo. Neuron. 2002; 34:437–446. [PubMed: 11988174]

Clarke S, Rivier F. Compartments within human primary auditory cortex: evidence from cytochrome oxidase and acetylcholinesterase staining. Eur J Neurosci. 1998; 10:741–745. [PubMed: 9749735]

Crone NE, Boatman D, Gordon B, Hao L. Induced electrocorticographic gamma activity during auditory perception. Clin Neurophysiol. 2001; 112:565–582. [PubMed: 11275528]

Crone NE, Sinai A, Korzeniewska A. High-frequency gamma oscillations and human brain mapping with electrocorticography. Prog Brain Res. 2006; 159:275–295. [PubMed: 17071238]

Da Costa S, van der Zwaag W, Marques JP, Frackowiak RS, Clarke S, Saenz M. Human primary auditory cortex follows the shape of Heschl's gyrus. J Neurosci. 2011; 31:14067–14075. [PubMed: 21976491]

Dang-Vu TT, Bonjean M, Schabus M, Boly M, Darsaud A, Desseilles M, Degueldre C, Balteau E, Phillips C, Luxen A, Sejnowski TJ, Maquet P. Interplay between spontaneous and induced brain

Author Manuscript Author Manuscript Author Manuscript Author Manuscript

activity during human non-rapid eye movement sleep. Proc Natl Acad Sci U S A. 2011; 108:15438–15443. [PubMed: 21896732]

Davis MH, Coleman MR, Absalom AR, Rodd JM, Johnsrude IS, Matta BF, Owen AM, Menon DK. Dissociating speech perception and comprehension at reduced levels of awareness. Proc Natl Acad Sci U S A. 2007; 104:16032–16037. [PubMed: 17938125]

De Cosmo G, Aceto P, Clemente A, Congedo E. Auditory evoked potentials. Minerva Anestesiol. 2004; 70:293–297. [PubMed: 15181406]

de la Mothe LA, Blumell S, Kajikawa Y, Hackett TA. Thalamic connections of the auditory cortex in marmoset monkeys: core and medial belt regions. J Comp Neurol. 2006; 496:72–96. [PubMed: 16528728]

De Martino F, Moerel M, Xu J, van de Moortele PF, Ugurbil K, Goebel R, Yacoub E, Formisano E. High-Resolution Mapping of Myeloarchitecture In Vivo: Localization of Auditory Areas in the Human Brain. Cereb Cortex. 2015; 25:3394–3405. [PubMed: 24994817]

Destrieux C, Fischl B, Dale A, Halgren E. Automatic parcellation of human cortical gyri and sulci using standard anatomical nomenclature. Neuroimage. 2010; 53:1–15. [PubMed: 20547229]

Dueck MH, Petzke F, Gerbershagen HJ, Paul M, Hesselmann V, Girnus R, Krug B, Sorger B, Goebel R, Lehrke R, Sturm V, Boerner U. Propofol attenuates responses of the auditory cortex to acoustic stimulation in a dose-dependent manner: a FMRI study. Acta Anaesthesiol Scand. 2005; 49:784–791. [PubMed: 15954960]

Dutton RC, Smith WD, Rampil IJ, Chortkoff BS, Eger EI. Forty-hertz midlatency auditory evoked potential activity predicts wakeful response during desflurane and propofol anesthesia in volunteers. Anesthesiology. 1999; 91:1209–1220. [PubMed: 10551569]

Edwards E, Soltani M, Kim W, Dalal SS, Nagarajan SS, Berger MS, Knight RT. Comparison of time-frequency responses and the event-related potential to auditory speech stimuli in human cortex. J Neurophysiol. 2009; 102:377–386. [PubMed: 19439673]

Eggermont JJ, Ponton CW. The neurophysiology of auditory perception: from single units to evoked potentials. Audiol Neurootol. 2002; 7:71–99. [PubMed: 12006736]

Eliades SJ, Crone NE, Anderson WS, Ramadoss D, Lenz FA, Boatman-Reich D. Adaptation of high-gamma responses in human auditory association cortex. J Neurophysiol. 2014; 112:2147–2163. [PubMed: 25122702]

Ellerkmann RK, Liermann VM, Alves TM, Wenningmann I, Kreuer S, Wilhelm W, Roepcke H, Hoeft A, Bruhn J. Spectral entropy and bispectral index as measures of the electroencephalographic effects of sevoflurane. Anesthesiology. 2004; 101:1275–1282. [PubMed: 15564933]

Faugeras F, Rohaut B, Weiss N, Bekinschtein T, Galanaud D, Puybasset L, Bolgert F, Sergent C, Cohen L, Dehaene S, Naccache L. Event related potentials elicited by violations of auditory regularities in patients with impaired consciousness. Neuropsychologia. 2012; 50:403–418. [PubMed: 22230230]

Fishman YI, Reser DH, Arezzo JC, Steinschneider M. Complex tone processing in primary auditory cortex of the awake monkey. I. Neural ensemble correlates of roughness. J Acoust Soc Am. 2000; 108:235–246. [PubMed: 10923888]

Formisano E, Kim DS, Di Salle F, van de Moortele PF, Ugurbil K, Goebel R. Mirror-symmetric tonotopic maps in human primary auditory cortex. Neuron. 2003; 40:859–969. [PubMed: 14622588]

Franks NP. General anaesthesia: from molecular targets to neuronal pathways of sleep and arousal. Nat Rev Neurosci. 2008; 9:370–386. [PubMed: 18425091]

Friston K. A theory of cortical responses. Philos Trans R Soc Lond B Biol Sci. 2005; 360:815–836. [PubMed: 15937014]

Fullerton BC, Pandya DN. Architectonic analysis of the auditory-related areas of the superior temporal region in human brain. J Comp Neurol. 2007; 504:470–498. [PubMed: 17701981]

Galaburda AM, Sanides F. Cytoarchitectonic organization of the human auditory cortex. J Comp Neurol. 1980; 190:597–610. [PubMed: 6771305]

Gemma M, de Vitis A, Baldoli C, Calvi MR, Blasi V, Scola E, Nobile L, Iadanza A, Scotti G, Beretta L. Functional magnetic resonance imaging (fMRI) in children sedated with propofol or midazolam. J Neurosurg Anesthesiol. 2009; 21:253–258. [PubMed: 19543005]

Author Manuscript Author Manuscript Author Manuscript Author Manuscript

Hackett, TA. Organization and correspondence of the auditory cortex of humans and nonhuman primates. In: Kaas, JH., editor. Evolution of Nervous Systems Vol. 4: Primates. Academic Press; New York: 2007. p. 109-119.

Hackett TA. Anatomic organization of the auditory cortex. Handb Clin Neurol. 2015; 129:27–53. [PubMed: 25726261]

Hackett TA, Stepniewska I, Kaas JH. Subdivisions of auditory cortex and ipsilateral cortical connections of the parabelt auditory cortex in macaque monkeys. J Comp Neurol. 1998; 394:475–95. [PubMed: 9590556]

Hackett TA, Preuss TM, Kaas JH. Architectonic identification of the core region in auditory cortex of macaques, chimpanzees, and humans. J Comp Neurol. 2001; 441:197–222. [PubMed: 11745645]

Hackett TA, De La Mothe LA, Ulbert I, Karmos G, Smiley J, Schroeder CE. Multisensory convergence in auditory cortex, II. Thalamocortical connections of the caudal superior temporal plane. J Comp Neurol. 2007; 502:924–952. [PubMed: 17444488]

Hashikawa T, Molinari M, Rausell E, Jones EG. Patchy and laminar terminations of medial geniculate axons in monkey auditory cortex. J Comp Neurol. 1995; 362:195–208. [PubMed: 8576433]

Heinke W, Fiebach CJ, Schwarzbauer C, Meyer M, Olthoff D, Alter K. Sequential effects of propofol on functional brain activation induced by auditory language processing: an event-related functional magnetic resonance imaging study. Br J Anaesth. 2004; 92:641–650. [PubMed: 15064248]

Howard MA, Volkov IO, Abbas PJ, Damasio H, Ollendieck MC, Granner MA. A chronic microelectrode investigation of the tonotopic organization of human auditory cortex. Brain Res. 1996; 724:260–264. [PubMed: 8828578]

Howard MA, Volkov IO, Mirsky R, Garell PC, Noh MD, Granner M, Damasio H, Steinschneider M, Reale RA, Hind JE, Brugge JF. Auditory cortex on the posterior superior temporal gyrus of human cerebral cortex. J Comp Neurol. 2000; 416:76–92.

Humphries C, Liebenthal E, Binder JR. Tonotopic organization of human auditory cortex. Neuroimage. 2010; 50:1202–1211. [PubMed: 20096790]

Huotari AM, Koskinen M, Suominen K, Alahuhta S, Remes R, Hartikainen KM, Jäntti V. Evoked EEG patterns during burst suppression with propofol. Br J Anaesth. 2004; 92:18–24. [PubMed: 14665548]

Iannuzzi M, Iannuzzi E, Chiefari M, Berrino L, Rossi F, Bonhomme VL, Hans PC. Bispectral index and state entropy of the electroencephalogram during propofol anaesthesia. Brit J Anaesth. 2007; 98:145. [PubMed: 17158130]

Jenison RL, Reale RA, Armstrong AL, Oya H, Kawasaki H, Howard MA 3rd. Sparse Spectro-Temporal Receptive Fields Based on Multi-Unit and High-Gamma Responses in Human Auditory Cortex. PLoS One. 2015; 10:e0137915. [PubMed: 26367010]

Jordan D, Ilg R, Riedl V, Schorer A, Grimberg S, Neufang S, Omerovic A, Berger S, Untergehrer G, Preibisch C, Schulz E, Schuster T, Schroter M, Spoormaker V, Zimmer C, Hemmer B, Wohlschlager A, Kochs EF, Schneider G. Simultaneous electroencephalographic and functional magnetic resonance imaging indicate impaired cortical top-down processing in association with anesthetic-induced unconsciousness. Anesthesiology. 2013; 119:1031–1042. [PubMed: 23969561]

Kaas JH, Hackett TA. Subdivisions of auditory cortex and processing streams in primates. Proc Natl Acad Sci U S A. 2000; 97:11793–11799. [PubMed: 11050211]

Kaas, JH., Hackett, TA. Subdivisions and connections of auditory cortex in primates: A working model. In: Konig, R.Heil, P.Budinger, E., Scheich, H., editors. Auditory cortex. A Synthesis of Human and Animal Research. Vol. 2005. Lawrence Erlbaum Associates; Mahwah, NJ: 2005. p. 7-26.

Kajikawa Y, de La Mothe L, Blumell S, Hackett TA. A comparison of neuron response properties in areas A1 and CM of the marmoset monkey auditory cortex: tones and broadband noise. J Neurophysiol. 2005; 93:22–34. [PubMed: 15342713]

Kiang NY, Moxon EC. Tails of tuning curves of auditory-nerve fibers. J Acoust Soc Am. 1974; 55:620–630. [PubMed: 4819862]

Kovach CK, Gander PE. The demodulated band transform. J Neurosci Methods. 2016; 261:135–154. [PubMed: 26711370]

Author Manuscript Author Manuscript Author Manuscript Author Manuscript

Langers DR, van Dijk P. Mapping the tonotopic organization in human auditory cortex with minimally salient acoustic stimulation. Cereb Cortex. 2012; 22:2024–2038. [PubMed: 21980020]

Liegeois-Chauvel C, Musolino A, Chauvel P. Localization of the primary auditory area in man. Brain. 1991; 114:139–151. [PubMed: 1900211]

Liégeois-Chauvel C, Musolino A, Badier JM, Marquis P, Chauvel P. Evoked potentials recorded from the auditory cortex in man: evaluation and topography of the middle latency components. Electroencephalogr Clin Neurophysiol. 1994; 92:204–214. [PubMed: 7514990]

Liégeois-Chauvel C, Lorenzi C, Trébuchon A, Régis J, Chauvel P. Temporal envelope processing in the human left and right auditory cortices. Cereb Cortex. 2004; 14:731–740. [PubMed: 15054052]

Liu X, Lauer KK, Ward BD, Rao SM, Li SJ, Hudetz AG. Propofol disrupts functional interactions between sensory and high-order processing of auditory verbal memory. Hum Brain Mapp. 2011; 33:2487–2498. [PubMed: 21932265]

Liu X, Lauer KK, Ward BD, Li SJ, Hudetz AG. Differential effects of deep sedation with propofol on the specific and nonspecific thalamocortical systems: a functional magnetic resonance imaging study. Anesthesiology. 2013; 118:59–69. [PubMed: 23221862]

Logothetis NK, Leopold DA, Sheinberg DL. What is rivalling during binocular rivalry? Nature. 2014; 380:621–624.

Mahon P, Kowalski RG, Fitzgerald AP, Lynch EM, Boylan GB, McNamara B, Shorten GD. Spectral entropy as a monitor of depth of propofol induced sedation. J Clin Monit Comput. 2008; 22:87–93. [PubMed: 18253846]

Mashour GA. Top-down mechanisms of anesthetic-induced unconsciousness. Front Syst Neurosci. 2014; 8:115. [PubMed: 25002838]

Merzenich MM, Brugge JF. Representation of the cochlear partition of the superior temporal plane of the macaque monkey. Brain Res. 1973; 50:275–296. [PubMed: 4196192]

Mesgarani N, Chang EF. Selective cortical representation of attended speaker in multi-talker speech perception. Nature. 2012; 485:233–236. [PubMed: 22522927]

Moerel M, De Martino F, Santoro R, Ugurbil K, Goebel R, Yacoub E, Formisano E. Processing of natural sounds: characterization of multipeak spectral tuning in human auditory cortex. J Neurosci. 2013; 33:11888–11898. [PubMed: 23864678]

Moerel M, De Martino F, Formisano E. An anatomical and functional topography of human auditory cortical areas. Front Neurosci. 2014; 8:225. [PubMed: 25120426]

Molinari M, Dell'Anna ME, Rausell E, Leggio MG, Hashikawa T, Jones EG. Auditory thalamocortical pathways defined in monkeys by calcium binding protein immunoreactivity. J Comp Neurol. 1995; 362:171–194. [PubMed: 8576432]

Morel A, Garraghty PE, Kaas JH. Tonotopic organization, architectonic fields, and connections of auditory cortex in macaque monkeys. J Comp Neurol. 1993; 335:437–459. [PubMed: 7693772]

Morosan P, Rademacher J, Schleicher A, Amunts K, Schormann T, Zilles K. Human primary auditory cortex: cytoarchitectonic subdivisions and mapping into a spatial reference system. Neuroimage. 2001; 13:684–701. [PubMed: 11305897]

Mukamel R, Fried I. Human intracranial recordings and cognitive neuroscience. Annu Rev Psychol. 2012; 63:511–537. [PubMed: 21943170]

Müller-Preuss P, Mitzdorf U. Functional anatomy of the inferior colliculus and the auditory cortex: current source density analyses of click-evoked potentials. Hear Res. 1984; 16:133–142. [PubMed: 6526745]

Murphy M, Bruno MA, Riedner BA, Boveroux P, Noirhomme Q, Landsness EC, Brichant JF, Phillips C, Massimini M, Laureys S, Tononi G, Boly M. Propofol anesthesia and sleep: a high-density EEG study. Sleep. 2011; 34:283–291A. [PubMed: 21358845]

Nagahama Y, Kovach CK, Ciliberto M, Joshi C, Rhone AE, Vesole A, Gander PE, Nourski KV, Oya H, Kawasaki H, Howard MA, Dlouhy BJ. Musicogenic epilepsy localizes to Heschl's gyrus and superior temporal plane. (in review).

Nourski KV, Brugge JF. Representation of temporal sound features in the human auditory cortex. Rev Neurosci. 2011; 22:187–203. [PubMed: 21476940]

Nourski KV, Howard MA 3rd. Invasive recordings in the human auditory cortex. Handb Clin Neurol 2015. 2015; 129:225–44.

Author Manuscript Author Manuscript Author Manuscript Author Manuscript

Nourski KV, Brugge JF, Reale RA, Kovach CK, Oya H, Kawasaki H, Jenison RL, Howard MA III. Coding of repetitive transients by auditory cortex on posterolateral superior temporal gyrus in humans: an intracranial electrophysiology study. J Neurophysiol. 2013; 109:1283–1295. [PubMed: 23236002]

Nourski KV, Steinschneider M, McMurray B, Kovach CK, Oya H, Kawasaki H, Howard MA 3rd. Functional organization of human auditory cortex: investigation of response latencies through direct recordings. Neuroimage. 2014; 101:598–609. [PubMed: 25019680]

Nourski KV, Steinschneider M, Oya H, Kawasaki H, Howard MA 3rd. Modulation of response patterns in human auditory cortex during a target detection task: an intracranial electrophysiology study. Int J Psychophysiol. 2015; 95:191–201. [PubMed: 24681353]

O'Connell MN, Barczak A, Ross D, McGinnis T, Schroeder CE, Lakatos P. Multi-Scale Entrainment of Coupled Neuronal Oscillations in Primary Auditory Cortex. Front Hum Neurosci. 2015; 9:655. [PubMed: 26696866]

Plourde G. The effects of propofol on the 40-Hz auditory steady-state response and on the electroencephalogram in humans. Anesth Analg. 1996; 82:1015–1022. [PubMed: 8610859]

Plourde G, Belin P, Chartrand D, Fiset P, Backman SB, Xie G, Zatorre RJ. Cortical processing of complex auditory stimuli during alterations of consciousness with the general anesthetic propofol. Anesthesiology. 2006; 104:448–457. [PubMed: 16508391]

Pockett S. Anesthesia and the electrophysiology of auditory consciousness. Conscious Cogn. 1999; 8:45–61. [PubMed: 10072693]

Portas CM, Krakow K, Allen P, Josephs O, Armony JL, Frith CD. Auditory processing across the sleep-wake cycle: simultaneous EEG and fMRI monitoring in humans. Neuron. 2000; 28:991–999. [PubMed: 11163282]

Rademacher J, Morosan P, Schormann T, Schleicher A, Werner C, Freund HJ, Zilles K. Probabilistic mapping and volume measurement of human primary auditory cortex. Neuroimage. 2001; 13:669–683. [PubMed: 11305896]

Ratnakumari L, Hemmings HC Jr. Effects of propofol on sodium channel-dependent sodium influx and glutamate release in rat cerebrocortical synaptosomes. Anesthesiology. 1997; 86:428–439. [PubMed: 9054261]

Rauschecker JP, Tian B, Hauser M. Processing of complex sounds in the macaque nonprimary auditory cortex. Science. 1995; 268:111–114. [PubMed: 7701330]

Ray S, Niebur E, Hsiao SS, Sinai A, Crone NE. High-frequency gamma activity (80–150Hz) is increased in human cortex during selective attention. Clin Neurophysiol. 2008; 119:116–133. [PubMed: 18037343]

Raz A, Grady SM, Krause BM, Uhlrich DJ, Manning KA, Banks MI. Preferential effect of isoflurane on top-down vs. bottom-up pathways in sensory cortex. Front Syst Neurosci. 2014; 8:191. [PubMed: 25339873]

Recanzone GH, Cohen YE. Serial and parallel processing in the primate auditory cortex revisited. Behav Brain Res. 2010; 206:1–7. [PubMed: 19686779]

Recanzone GH, Guard DC, Phan ML, Su TK. Correlation between the activity of single auditory cortical neurons and sound-localization behavior in the macaque monkey. J Neurophysiol. 2000; 83:2723–2739. [PubMed: 10805672]

Reddy CG, Dahdaleh NS, Albert G, Chen F, Hansen D, Nourski K, Kawasaki H, Oya H, Howard MA III. A method for placing Heschl gyrus depth electrodes. J Neurosurg. 2010; 112:1301–1307. [PubMed: 19663547]

Rivier F, Clarke S. Cytochrome oxidase, acetylcholinesterase, and NADPH-diaphorase staining in human supratemporal and insular cortex: evidence for multiple auditory areas. Neuroimage. 1997; 6:288–304. [PubMed: 9417972]

Rudolph U, Antkowiak B. Molecular and neuronal substrates for general anaesthetics. Nat Rev Neurosci. 2004; 5:709–720. [PubMed: 15322529]

Sacco CB, Tardif E, Genoud C, Probst A, Tolnay M, Janzer RC, Verney C, Kraftsik R, Clarke S. GABA receptor subunits in human auditory cortex in normal and stroke cases. Acta Neurobiol Exp (Wars). 2009; 69:469–493. [PubMed: 20048764]

Author Manuscript Author Manuscript Author Manuscript Author Manuscript

Saenz M, Langers DR. Tonotopic mapping of human auditory cortex. Hear Res. 2014; 307:42–52. [PubMed: 23916753]

Scheller B, Schneider G, Daunderer M, Kochs EF, Zwissler B. High-frequency components of auditory evoked potentials are detected in responsive but not in unconscious patients. Anesthesiology. 2005; 103:944–950. [PubMed: 16249667]

Schmidt GN, Bischoff P, Standl T, Hellstern A, Teuber O, Schulte Esch J. Comparative evaluation of the Datex-Ohmeda S/5 Entropy Module and the Bispectral Index monitor during propofol-remifentanil anesthesia. Anesthesiology. 2004; 101:1283–1290. [PubMed: 15564934]

Schnider TW, Minto CF, Gambus PL, Andresen C, Goodale DB, Shafer SL, Youngs EJ. The influence of method of administration and covariates on the pharmacokinetics of propofol in adult volunteers. Anesthesiology. 1998; 88:1170–1182. [PubMed: 9605675]

Schnider TW, Minto CF, Shafer SL, Gambus PL, Andresen C, Goodale DB, Youngs EJ. The influence of age on propofol pharmacodynamics. Anesthesiology. 1999; 90:1502–1516. [PubMed: 10360845]

Schroeder CE, Tenke CE, Givre SJ, Arezzo JC, Vaughan HG Jr. Striate cortical contribution to the surface-recorded pattern-reversal VEP in the alert monkey. Vision Res. 1981; 23:1143–1157.

Schroter MS, Spoormaker VI, Schorer A, Wohlschlager A, Czisch M, Kochs EF, Zimmer C, Hemmer B, Schneider G, Jordan D, Ilg R. Spatiotemporal reconfiguration of large-scale brain functional networks during propofol-induced loss of consciousness. J Neurosci. 2012; 32:12832–12840. [PubMed: 22973006]

Schrouff J, Perlbarg V, Boly M, Marrelec G, Boveroux P, Vanhaudenhuyse A, Bruno MA, Laureys S, Phillips C, Pelegrini-Issac M, Maquet P, Benali H. Brain functional integration decreases during propofol-induced loss of consciousness. Neuroimage. 2011; 57:198–205. [PubMed: 21524704]

Schwender D, Daunderer M, Mulzer S, Klasing S, Finsterer, Peter K. Midlatency auditory evoked potentials predict movements during anesthesia with isoflurane or propofol. Anesth Analg. 1997; 85:164–173. [PubMed: 9212142]

Schwilden H, Kochs E, Daunderer M, Jeleazcov Ch, Scheller B, Schneider G, Schüttler J, Schwender D, Stockmanns G, Pöppel E. Concurrent recording of AEP, SSEP and EEG parameters during anaesthesia: a factor analysis. Br J Anaesth. 2005; 95:197–206. [PubMed: 15980046]

Simpson TP, Manara AR, Kane NM, Barton RL, Rowlands CA, Butler SR. Effect of propofol anaesthesia on the event-related potential mismatch negativity and the auditory-evoked potential N1. Br J Anaesth. 2002; 89:382–388. [PubMed: 12402715]

Steinschneider M, Tenke CE, Schroeder CE, Javitt DC, Simpson GV, Arezzo JC, Vaughan HG Jr. Cellular generators of the cortical auditory evoked potential initial component. Electroencephalogr Clin Neurophysiol. 1992; 84:196–200. [PubMed: 1372236]

Steinschneider M, Schroeder CE, Arezzo JC, Vaughan HG Jr. Speech-evoked activity in primary auditory cortex: effects of voice onset time. Electroencephalogr Clin Neurophysiol. 1994; 92:30–43. [PubMed: 7508851]

Steinschneider M, Reser DH, Fishman YI, Schroeder CE, Arezzo JC. Click train encoding in primary auditory cortex of the awake monkey: evidence for two mechanisms subserving pitch perception. J Acoust Soc Am. 1998; 104:2935–2955. [PubMed: 9821339]

Steinschneider M, Fishman YI, Arezzo JC. Spectrotemporal analysis of evoked and induced electroencephalographic responses in primary auditory cortex (A1) of the awake monkey. Cereb Cortex. 2008; 18:610–625. [PubMed: 17586604]

Strauss M, Sitt JD, King JR, Elbaz M, Azizi L, Buiatti M, Naccache L, van Wassenhove V, Dehaene S. Disruption of hierarchical predictive coding during sleep. Proc Natl Acad Sci U S A. 2015; 112:E1353–62. [PubMed: 25737555]

Striem-Amit E, Hertz U, Amedi A. Extensive cochleotopic mapping of human auditory cortical fields obtained with phase-encoding FMRI. PLoS One. 2011; 6:e17832. [PubMed: 21448274]

Sullivan EM, Timi P, Hong LE, O'Donnell P. Effects of NMDA and GABA-A Receptor Antagonism on Auditory Steady-State Synchronization in Awake Behaving Rats. Int J Neuropsychopharmacol. 2015; 18:pyu118. [PubMed: 25556198]

Author Manuscript Author Manuscript Author Manuscript Author Manuscript

Sutter ML. Shapes and level tolerances of frequency tuning curves in primary auditory cortex: quantitative measures and population codes. J Neurophysiol. 2000; 84:1012–1025. [PubMed: 10938324]

Sweet RA, Dorph-Petersen KA, Lewis DA. Mapping auditory core, lateral belt, and parabelt cortices in the human superior temporal gyrus. J Comp Neurol. 2005; 491:270–289. [PubMed: 16134138]

Talavage TM, Ledden PJ, Benson RR, Rosen BR, Melcher JR. Frequency-dependent responses exhibited by multiple regions in human auditory cortex. Hear Res. 2000; 150:225–244. [PubMed: 11077206]

Talavage TM, Sereno MI, Melcher JR, Ledden PJ, Rosen BR, Dale AM. Tonotopic organization in human auditory cortex revealed by progressions of frequency sensitivity. J Neurophysiol. 2004; 91:1282–1296. [PubMed: 14614108]

Tong F. Primary visual cortex and visual awareness. Nat Rev Neurosci. 2003; 4:219–229. [PubMed: 12612634]

Tononi G. An information integration theory of consciousness. BMC Neurosci. 2004; 5:42. [PubMed: 15522121]

Vakkuri A, Yli-Hankala A, Talja P, Mustola S, Tolvanen-Laakso H, Sampson T, Viertiö-Oja H. Time-frequency balanced spectral entropy as a measure of anesthetic drug effect in central nervous system during sevoflurane, propofol, and thiopental anesthesia. Acta Anaesthesiol Scand. 2004; 48:145–153. [PubMed: 14995935]

Vanluchene AL, Vereecke H, Thas O, Mortier EP, Shafer SL, Struys MM. Spectral entropy as an electroencephalographic measure of anesthetic drug effect: a comparison with bispectral index and processed midlatency auditory evoked response. Anesthesiology. 2004; 101:34–42. [PubMed: 15220769]

Velly LJ, Rey MF, Bruder NJ, Gouvitsos FA, Witjas T, Regis JM, Peragut JC, Gouin FM. Differential dynamic of action on cortical and subcortical structures of anesthetic agents during induction of anesthesia. Anesthesiology. 2007; 107:202–212. [PubMed: 17667563]

Viertiö-Oja H, Maja V, Särkelä M, Talja P, Tenkanen N, Tolvanen-Laakso H, Paloheimo M, Vakkuri A, Yli-Hankala A, Meriläinen P. Description of the Entropy algorithm as applied in the Datex-Ohmeda S/5 Entropy Module. Acta Anaesthesiol Scand. 2004; 48:154–161. [PubMed: 14995936]

Von Economo C, Horn L. Uber Windungsrelief, Masse und Rindenarchitektonik der Supratemporalflache, ihre individuellen und ihre Seitenunterschiede. Z Neurol Psychiatr. 1930; 130:678–757.

Von Economo, C., Koskinas, G. Die Cytoarchitectonik der Hirnrinde des erwachsenen menschen. Julius-Springer; Berlin: 1925.

Wallace MN, Johnston PW, Palmer AR. Histochemical identification of cortical areas in the auditory region of the human brain. Exp Brain Res. 2002; 143:499–508. [PubMed: 11914796]

Wasserthal C, Brechmann A, Stadler J, Fischl B, Engel K. Localizing the human primary auditory cortex in vivo using structural MRI. Neuroimage. 2014; 93:237–251. [PubMed: 23891882]

Watanabe M, Cheng K, Murayama Y, Ueno K, Asamizuya T, Tanaka K, Logothetis N. Attention but not awareness modulates the BOLD signal in the human V1 during binocular suppression. 2011; 334:829–331.

Woods DL, Stecker GC, Rinne T, Herron TJ, Cate AD, Yund EW, Liao I, Kang X. Functional maps of human auditory cortex: effects of acoustic features and attention. PLoS One. 2009; 4:e5183. [PubMed: 19365552]

Woods DL, Herron TJ, Cate AD, Yund EW, Stecker GC, Rinne T, Kang X. Functional properties of human auditory cortical fields. Front Syst Neurosci. 2010; 4:155. [PubMed: 21160558]

Yang J, Wang W, Yong Z, Weidong M, Zhang H. Propofol differentially inhibits the release of glutamate, γ-aminobutyric acid and glycine in the spinal dorsal horn of rats. Iran J Basic Med Sci. 2015; 18: 822–826. [PubMed: 26557972]

Yvert B, Fischer C, Bertrand O, Pernier J. Localization of human supratemporal auditory areas from intracerebral auditory evoked potentials using distributed source models. Neuroimage. 2005; 28:140–153. [PubMed: 16039144]

Author Manuscript Author Manuscript Author Manuscript Author Manuscript

Zilles K, Schleicher A, Langemann C, Amunts K, Morosan P, Palomero-Gallagher N, Schormann T, Mohlberg H, Bürgel U, Steinmetz H, Schlaug G, Roland PE. Quantitative analysis of sulci in the human cerebral cortex: development, regional heterogeneity, gender difference, asymmetry, intersubject variability and cortical architecture. Hum Brain Mapp. 2007; 5:218–221.

Author Manuscript Author Manuscript Author Manuscript Author Manuscript

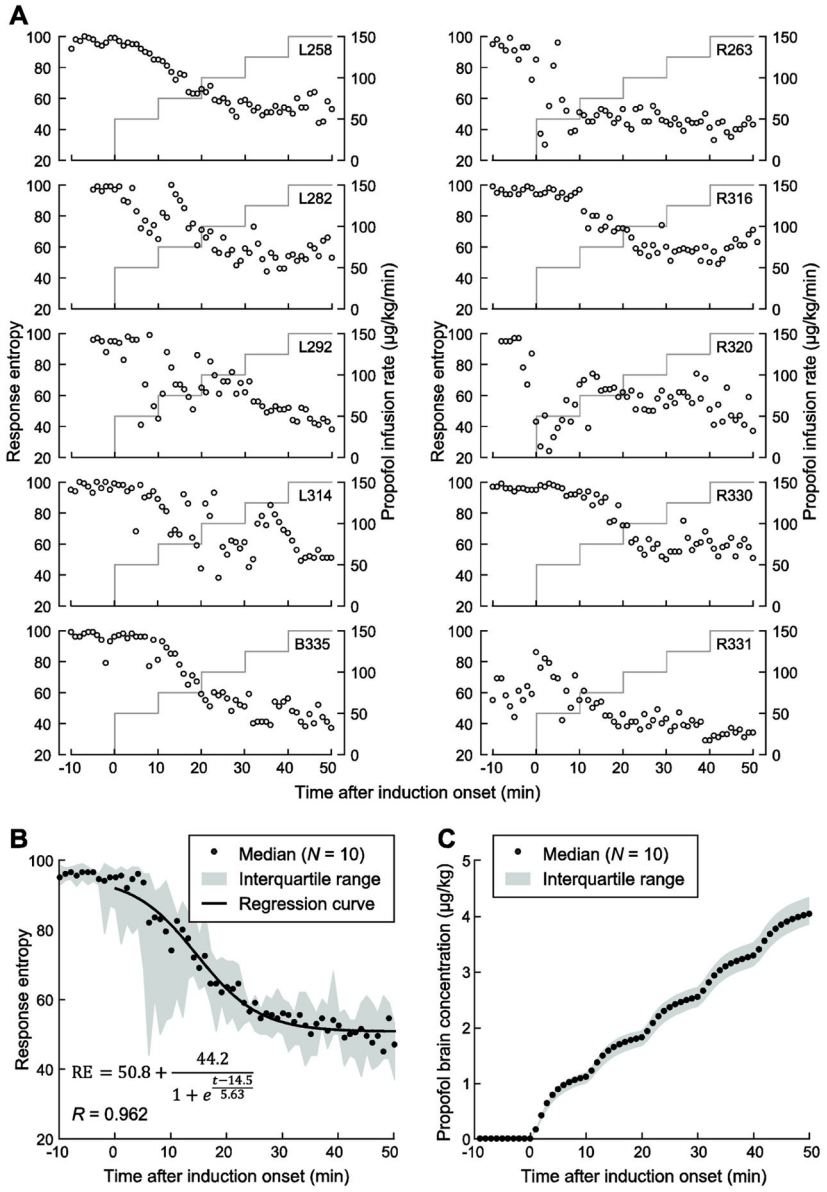

Figure 1.

Time course of propofol induction. **A**: Data from individual subjects. Propofol infusion rate (gray lines) and response entropy (RE; open circles) are plotted as functions of time after induction onset. **B**: Average time course of induction across all subjects. RE plotted as a function of time after induction onset. Median values are depicted as circles. Solid line represents sigmoidal regression curve fitted to the across-subject median RE values. **C:** Estimated propofol brain concentrations over the course of the experiment.

Author Manuscript Author Manuscript Author Manuscript Author Manuscript

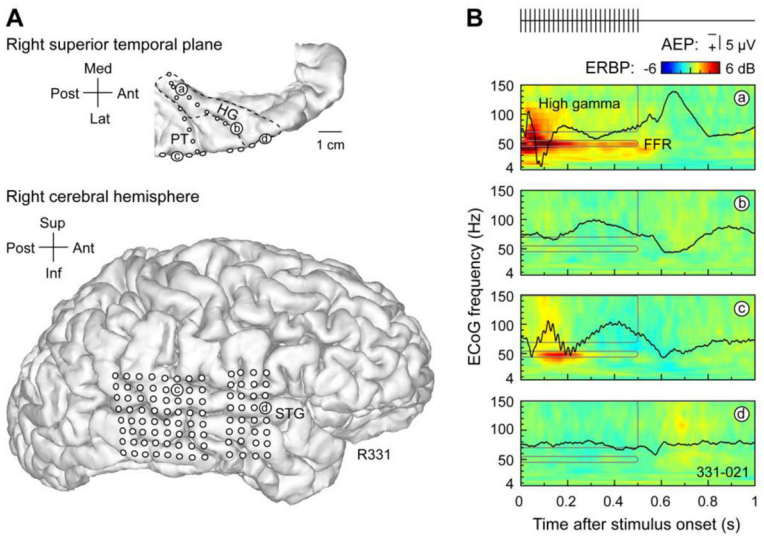

Figure 2.

Auditory cortical responses to click train stimuli. Exemplary data from subject R331. **A:** MRI top-down view of superior temporal plane and side view of the hemispheric surface showing the locations of chronically implanted depth (e.g. ‘a’ and ‘b’) and subdural (e.g. ‘c’ and ‘d’) electrodes, respectively. HG is denoted by a dashed line. **B:** Responses to the 50 Hz 500 ms click trains recorded from four representative auditory cortical sites (‘a’–‘d’) (‘a’: posteromedial HG; ‘b’: anterolateral HG; ‘c’: posterior STG; ‘d’: middle STG). AEP waveforms are depicted in black on top of ERBP time-frequency plots. Responses were averaged over the 10-minute interval prior to the initiation of propofol infusion. Time-frequency windows used for FFR and high gamma ERBP analysis are outlined in gray. Stimulus schematic is shown on top.

Author Manuscript Author Manuscript Author Manuscript Author Manuscript

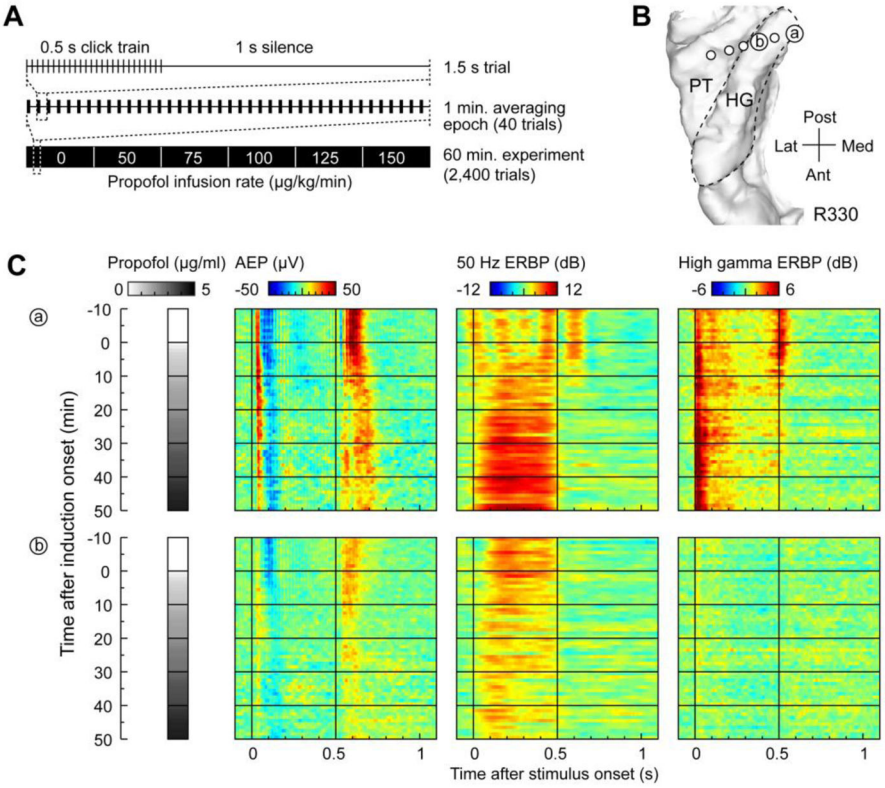

Figure 3.

Auditory cortical responses recorded from posteromedial HG during induction of propofol anesthesia. Exemplary data from subject R330. **A**: Experiment time course schematic. Single trial (1.5 s), 40-trial averaging epoch (1 min.) and the entire experiment (60 min.) are depicted on top, middle and bottom, respectively. **B**: MRI top-down view of superior temporal plane showing the location of chronically implanted depth electrode and two representative sites in posteromedial HG (‘a’ and ‘b’). HG is denoted by a dashed line. **C**: Time course of changes in AEP voltage, FFR (measured as ERBP at 50 Hz) and high gamma ERBP (left, middle and right color plots, respectively) recorded from sites ‘a’ and ‘b’ (top and bottom row, respectively). Each color plot represents a series of one-minute (40-trial) peristimulus averages, arranged according to time after induction onset (top to bottom). Grayscale bars represent propofol brain concentrations, estimated using pharmacokinetic and pharmacodynamic data (see Methods).

Author Manuscript Author Manuscript Author Manuscript Author Manuscript

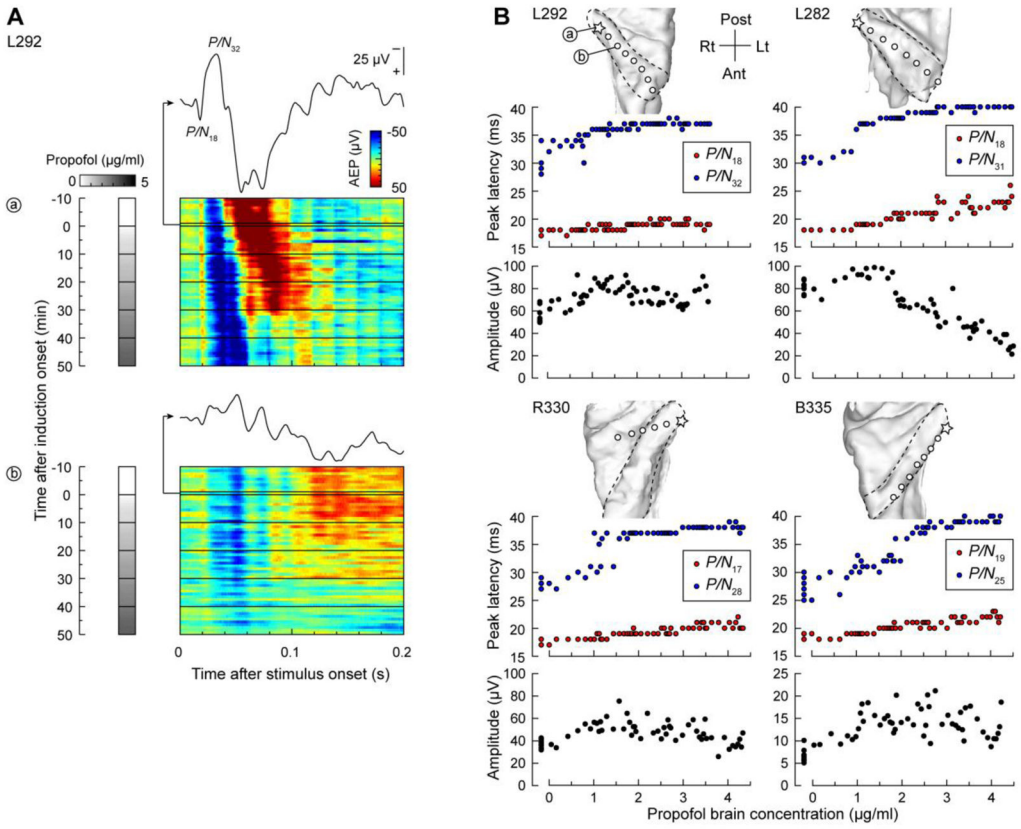

Figure 4.

Changes in the early AEP components recorded from HG during induction of propofol anesthesia. **A**: Time course of changes in AEP voltage recorded from two representative posteromedial HG sites (‘a’ and ‘b’) in subject L292. Each color plot represents a series of one-minute (40-trial) peristimulus averages, arranged according to time after induction onset (top to bottom). Grayscale bars represent estimated propofol brain concentrations. Exemplary AEP waveforms computed over the 1-minute interval immediately preceding induction onset are replotted above the color plots. P/N18 and P/N32 denote the two early AEP peaks. **B**: Latency (red and blue symbols) and amplitude (black symbols) of early AEP components plotted as functions of propofol brain concentration. AEPs were recorded from sites in the most posteromedial aspect of the gyrus in four subjects (location denoted by stars in the MRI top-down views of the superior temporal plane; HG is denoted in each subject by a dashed line). Measurements made during the first 9 minutes of the experiment prior to induction are offset on the X axis.

Author Manuscript Author Manuscript Author Manuscript Author Manuscript

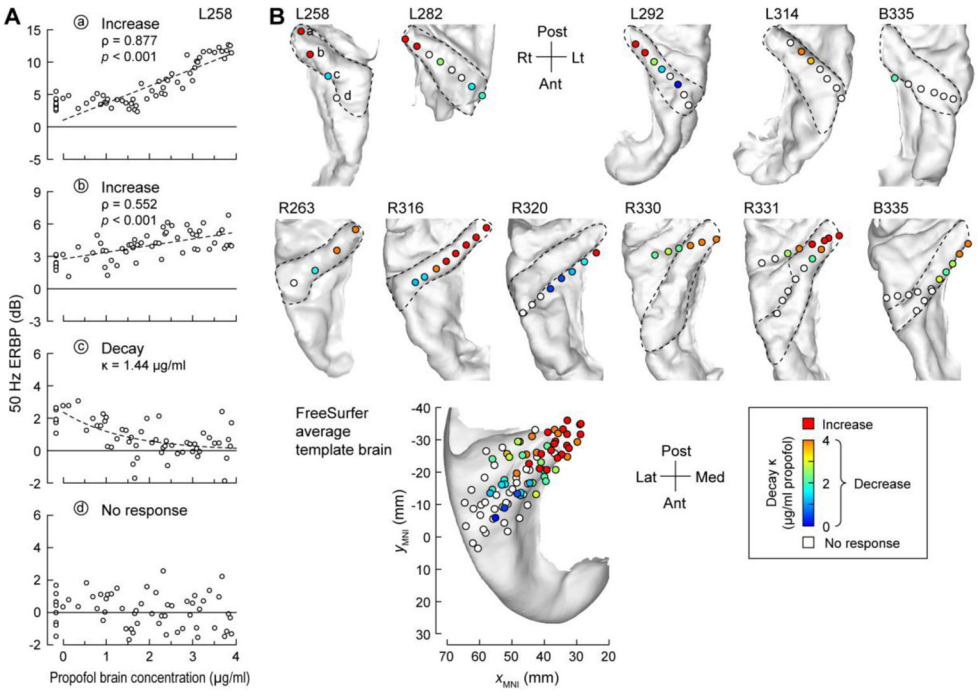

Figure 5.

Changes in FFR measured in HG during induction of propofol anesthesia. **A**: FFR (measured as ERBP at 50 Hz) plotted as functions of propofol brain concentration for four representative sites in subject L258 (‘a’–‘d’, top to bottom panels, respectively). Dashed lines represent linear regression (in ‘a’ and ‘b’) and exponential decay (in ‘c’) fits to the data. Measurements made during the first 9 minutes of the experiment prior to induction are offset on the X axis. **B**: Summary of FFR measurements from individual subjects. HG is denoted in each subject by a dashed line. Bottom panel: locations of recording sites plotted in MNI coordinate space and projected onto FreeSurfer average template brain.

Author Manuscript Author Manuscript Author Manuscript Author Manuscript

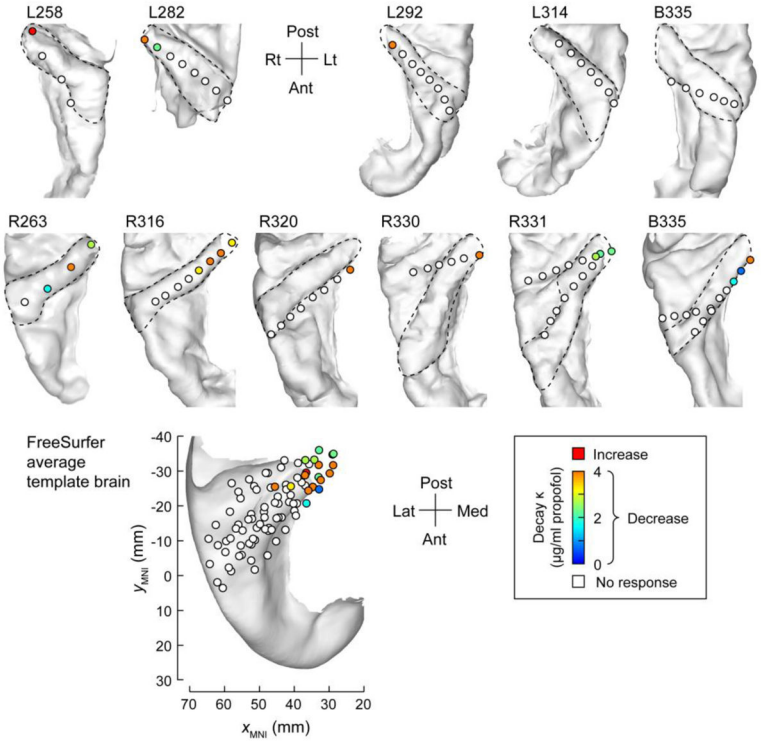

Figure 6.

Changes in high gamma ERBP measured in HG during induction of propofol anesthesia. See legend of Figure 5B for details.

Author Manuscript Author Manuscript Author Manuscript Author Manuscript

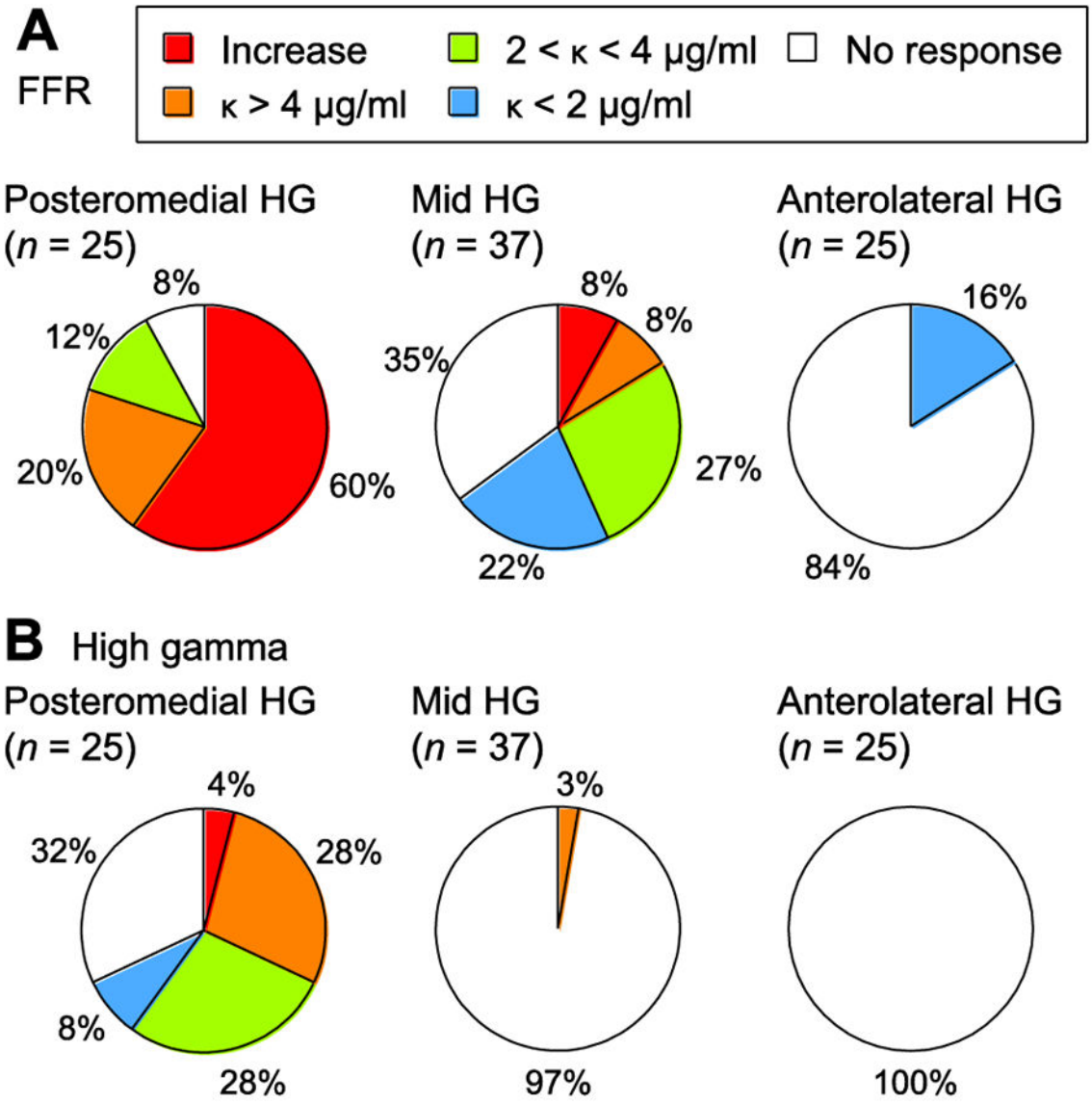

Figure 7.

Summary of changes in auditory cortical responses measured in HG during induction of propofol anesthesia. Pie charts show proportions of sites within posteromedial, mid and anterolateral sub-regions of HG that exhibited specific types of FFR and high gamma changes (panels **A** and **B**, respectively).

Author Manuscript Author Manuscript Author Manuscript Author Manuscript

Table 1

Subject demographics.

Subject code[1]	Age	Sex[2]	Handedness[3]	Language dominance[3]	Seizure focus	Surgical procedure
L258	38	M	R	L	Broad from L contacts, no discrete localization	No resection
R263	33	F	R	L	R inferior frontal gyrus (posterior ventral), anterior insula	Resection of R ventral frontal lobe and R anterior insula
L282	40	M	R	L	L posterior superior temporal, basal frontal	Resection of L posterior hippocampus, L amygdala and L posterior lateral basal frontal cortex
L292	50	F	L	R	L medial temporal, dorsal frontal	Resection of L anterior and medial temporal lobe and L medial dorsal frontal lobe
L314	31	F	R	L	R amygdala, L occipital lobe	No resection
R316	31	F	R	L	R medial temporal	Resection of R anterior and medial temporal lobe
R320	51	F	R	L	R medial temporal	Resection of R anterior and medial temporal lobe
R330	43	M	L	N/A	R occipital lobe	Resection of R occipital cortex
R331	35	M	R	N/A	Bilateral medial temporal	No resection
B335	33	M	R	L	Bilateral medial temporal	No resection

[1] Letter prefix of the subject code denotes the side of electrode implantation over the auditory cortex (L = left; R = right; B = both hemispheres). Most subjects had, to varying degrees, bilateral coverage of other regions of the brain.

[2] F = female; M = male

[3] L = left; R = right; N/A = Wada test not performed